Molecular Oncology

FEBS PRESS science publishing by scientists

β-Catenin in desmoid-type fibromatosis: deep insights into the role of T41A and S45F mutations on protein structure and gene expression

Chiara Colombo[1], Antonino Belfiore[2], Nicholas Paielli[2], Loris De Cecco[3], Silvana Canevari[3], Erik Laurini[4], Maurizio Fermeglia[4], Sabrina Pricl[4], Paolo Verderio[5], Stefano Bottelli[5], Marco Fiore[1], Silvia Stacchiotti[6], Elena Palassini[6], Alessandro Gronchi[1], Silvana Pilotti[2] and Federica Perrone[2]

1 Sarcoma Service, Department of Surgery, Fondazione IRCCS Istituto Nazionale Tumori, Milan, Italy
2 Laboratory of Experimental Molecular Pathology, Department of Pathology, Fondazione IRCCS Istituto Nazionale Tumori, Milan, Italy
3 Functional Genomics and Bioinformatics, Department of Applied Research and Technology Development, Fondazione IRCCS Istituto Nazionale dei Tumori, Milan, Italy
4 Molecular Simulation Engineering (MOSE) Laboratory, DEA, University of Trieste, Italy
5 Unit of Medical Statistics, Biometry and Bioinformatics, Fondazione IRCCS Istituto Nazionale Tumori, Milan, Italy
6 Adult Mesenchymal Tumor Medical Oncology Unit, Fondazione IRCCS Istituto Nazionale Tumori, Milan, Italy

Keywords
desmoid-type fibromatosis; gene expression; modeling; β-catenin mutation

Correspondence
C. Colombo, Sarcoma Service, Department of Surgery, Fondazione IRCCS Istituto Nazionale Tumori, G. Venezian 1, 20133 Milan, Italy
Fax: +39 02 2390 2404
Tel: +39 02 2390 3234
E-mail: chiara.colombo@istitutotumori.mi.it

(Received 10 April 2017, revised 30 May 2017, accepted 3 June 2017)

doi:10.1002/1878-0261.12101

Desmoid-type fibromatosis (DF) is a rare mesenchymal lesion with high risk of local recurrence. Specific β-catenin mutations (S45F) appeared to be related to this higher risk compared to T41A-mutated or wild-type (WT). We explored the influence of both mutations and WT on structure stability and affinity of β-catenin for α-catenin and the pattern of gene expression that may influence DF behavior. Using 33 surgically resected primary DFs harboring T41A (n = 14), S45F (n = 10), or WT (n = 9), we performed a comparative molecular analysis by protein/protein interaction modeling, gene expression by DASL microarrays, human inflammation gene panel, and assessment of immune system-based biomarkers by immunohistochemistry. Mutated proteins were more stable than WT and formed a weaker complex with α-catenin. Consensus unsupervised gene clustering revealed the presence of two DF group-mutated (T41A + S45F) and WT (P = 0.0047). The gene sets 'Inflammatory-Defense-Humoral Immune Response' and 'Antigen Binding' were significantly enriched in T41A. The deregulation of 16 inflammation-related genes was confirmed. Low numbers of T cells and tumor-associated macrophages (TAM) infiltrating the tumors and low/absent PD-1/PD-L1 expression were also identified. We demonstrated that mutated DFs (T41A or S45F) and WT are two distinct molecular subgroups with regard to β-catenin stability, α-catenin affinity, and gene expression profiling. A different inflammation signature characterized the two mutated groups, suggesting mediation either by T41A or by S45F. Finally, all mutated cases showed a low number of TIL and TAM cells and a low or absent expression of PD-1 and PD-L1 consistent with β-catenin activation insensitive to checkpoint blockade.

Abbreviations
ADL, average dynamic length; DF, desmoid-type fibromatosis; FDR, false discovery rate; FFPE, formalin-fixed paraffin-embedded; GSEA, gene set enrichment analysis; MD, molecular dynamics; NES, normalized enrichment score; n, number; PAR, progression arrest rate; RFS, recurrence-free survival; TAM, tumor-associated macrophages; TIL, tumor-infiltrating lymphocytes; WT, wild-type.

1. Introduction

Desmoid-type fibromatosis (DF) is a rare mesenchymal infiltrative lesion that exhibits high risk of local recurrence despite surgery with negative resection margins. The high propensity to relapse, the need for multiple surgeries with consequent functional and cosmetic impairment, the observation of prolonged stability in the absence of specific treatments, and the description of spontaneous regression have let the sarcoma community to change the management of this disease toward a more conservative tendency (Bonvalot *et al.*, 2008; Fiore *et al.*, 2009). Recently, guidelines have underlined the possibility of proposing a frontline observational approach to almost all patients with newly DF reserving specific treatments such as different drug regimens, radiotherapy, or surgery to selected cases including progressive disease (Kasper *et al.*, 2015). Unfortunately, changing in the clinical practice has not been paralleled by increasing knowledge regarding the pathogenesis and progression of this rare disease. Accurate molecular predictors that can be used at the beginning of the clinical history to tailor specific treatments are not available to date. Mutations in *CTNNB1* gene encoding for β-catenin are typically carried by most sporadic DFs. Three different β-catenin point mutations, T41A, S45F, and S45P, have been described in the vast majority of DFs and have been associated with the prevention of protein phosphorylation and subsequent protein stabilization with translocation to the nucleus, where β-catenin regulates transcription through its interaction with TCF/LEF (Kundu *et al.*, 2006). These β-catenin mutations were evaluated for their impact on DF patients' outcome. By comparing mutated and wild-type (WT) surgical DFs, we and other groups observed a statistically significant association between *CTNNB1* mutations and higher risk for local recurrence (van Broekhoven *et al.*, 2015; Colombo *et al.*, 2013; Dômont *et al.*, 2010). In particular, the specific mutation S45F was associated with worse recurrence-free survival (RFS) (van Broekhoven *et al.*, 2015; Colombo *et al.*, 2013; Lazar *et al.*, 2008). However, this evidence was not confirmed by other groups who reported a statistically not significant trend of poorer outcome in patients harboring the S45F mutation (Dômont *et al.*, 2010) or no correlation between the specific *CTNNB1* mutation and RFS (Mullen *et al.*, 2013; Romero *et al.*, 2012). Regarding the impact of mutations on response to medical treatment, Nishida *et al.* did not find a correlation between the efficacy of methotrexate or vinblastine and specific *CTNNB1* mutations (Nishida *et al.*, 2015). On the other hand, only the S45F mutation was significantly associated with a poor response to meloxicam (Hamada *et al.*, 2016) and with a progression arrest rate after imatinib treatment (Kasper *et al.*, 2016).

In this scenario of contrasting evidence of the impact of *CTNNB1* mutations and considering that these mutations map in the N-terminal domain of β-catenin that mediates both its degradation and interaction with α-catenin in the cell–cell adhesions (Jiang and Struhl, 1998; Pokutta *et al.*, 2014), we hypothesized that the mutation type could influence the stability of the β-catenin structure, its affinity for α-catenin, as well as the pattern of gene expression that in turn may guide the behavior of the disease. Thus, in this work, we performed a comparative molecular analysis of protein structure based on protein/protein interaction modeling and of gene and protein expression.

2. Materials and methods

2.1. Patients and samples

For this study, we selected 33 primary DFs surgically treated at our institution. All samples had the following characteristics: (a) DF diagnosis by an expert pathologist (SP); (b) known *CTNNB1* mutational status assessed by direct sequencing as previously described (Colombo *et al.*, 2013); (c) availability of the formalin-fixed paraffin-embedded (FFPE) surgical specimen; (d) availability of RNA amount and quality adequate for molecular analysis. The distribution of mutations was T41A (14 cases), S45F (10 cases), and WT (nine cases). Patients and disease characteristics are detailed in Table 1. Data retrieved were gender, age at surgery, anatomical site (abdominal wall, intra-abdominal, and extra-abdominal including extremity/girdle, head/neck, thoracic wall), size (cm), *CTNNB1* mutational status, data of surgery, data of recurrence, data of last follow-up, status at last follow-up. All patients had a macroscopically complete (including R0 and R1 margins) surgical resection except one. All samples were obtained after informed consent from patients. The study was approved by the Independent Ethics Committee of Fondazione IRCCS Istituto Nazionale dei Tumori (Approval Number RF-2009-1511297).

2.2. Modeling

The optimized full-length three-dimensional (3D) models of WT and mutant isoforms of β-catenin were obtained by a combination of homology modeling techniques with molecular dynamics (MD) refinements

Table 1. Patients and disease characteristics.

No.	Age (years)	Anatomical site	Size (cm)	CTNNB1 status	Recurrence	Margins	Adjuvant RT	Status at last follow-up
1	60	Extra-abdominal	4	T41A	NO	R1	Yes	NED
2	39	Abdominal wall	5	WT	NO	R0	No	NED
3	36	Abdominal wall	15	S45F	NO	R0	No	NED
4	32	Abdominal wall	5	T41A	NO	R0	No	NED
5	53	Extra-abdominal	12	S45F	15/03/2007	R0	Yes	AWD
6	49	Intra-abdominal	4	T41A	NO	R0	No	NED
7	16	Extra-abdominal	3	WT	NO	R0	No	NED
8	26	Extra-abdominal	2	WT	NO	R1	No	NED
9	19	Abdominal wall	10	S45F	NO	R0	No	NED
10	33	Extra-abdominal	5	T41A	NO	R1	No	NED
11	67	Extra-abdominal	4	WT	NO	R0	No	NED
12	42	Abdominal wall	6	S45F	NO	R0	No	NED
13	32	Abdominal wall	8	S45F	NO	R0	No	NED
14	25	Extra-abdominal	7	T41A	NO	R1	No	NED
15	69	Intra-abdominal	4	T41A	NO	R0	No	NED
16	39	Abdominal wall	6	WT	NO	R1	No	NED
17	70	Extra-abdominal	6	WT	NO	R0	No	NED
18	32	Extra-abdominal	5	T41A	YES	R1	No	NED
19	32	Abdominal wall	6	T41A	NO	R0	No	NED
20	17	Extra-abdominal	9	T41A	NO	R0	No	NED
21	28	Intra-abdominal	18	T41A	NO	R0	No	NED
22	33	Abdominal wall	10	S45F	NO	R0	No	NED
23	36	Extra-abdominal	5	WT	15/07/2006	R0	No	AWD
24	51	Extra-abdominal	–	T41A	NO	R1	No	NED
25	37	Intra-abdominal	28	WT	NO	R0	No	NED
26	25	Abdominal wall	15	WT	NO	R0	No	NED
27	47	Extra-abdominal	11	S45F	NO	R1	Yes	NED
28	31	Intra-abdominal	–	T41A	NO	R2	Yes	AWD
29	45	Intra-abdominal	3	T41A	NO	R0	No	DOC
30	43	Abdominal wall	7	T41A	NO	R0	No	NED
31	50	Extra-abdominal	7	S45F	NO	R0	No	NED
32	43	Extra-abdominal	11	S45F	3/05/2007	R1	No	AWD
33	24	Extra-abdominal	6	S45F	5/10/2005	R0	No	AWD

NED, not evidence of disease; AWD, alive with disease; DOC, dead for other cause.

(Bozzi *et al.*, 2013; Dileo *et al.*, 2011; Laurini *et al.*, 2011; Morgan *et al.*, 2015). WT and mutant β-catenin thermodynamic stability was determined by MD simulations in the molecular mechanics/Poisson Boltzmann surface area (MM/PBSA) framework of theory (Ferrone *et al.*, 2006; Gibbons *et al.*, 2014; Negri *et al.*, 2009; Pierotti *et al.*, 2010, 2011; Pricl *et al.*, 2015). The available structure of β-catenin (4IGG pdb) was used to build all WT and mutant β-catenin/α-catenin protein–protein complex and to determine the dynamics and energetics of their interactions via MM/PBSA MD simulations (see Data S1 for details).

2.3. RNA isolation and whole-genome gene expression profiling

The sample areas containing more than 90% tumor cells without necrosis or surrounding normal tissue were chosen for the analysis and macrodissected. Total RNA was isolated using Qiagen RNeasy FFPE Kit (Qiagen, Valencia, CA, USA) following the manufacturer's instructions and quantified by Nanodrop-1000 instrument (Thermo Fisher Scientific, Waltham, MA, USA). RNA quality was assessed by RT-qPCR amplifying amplicons of different size for ACTB housekeeping gene (Mittempergher *et al.*, 2011; Ravo *et al.*, 2008). Two hundred nanogram of RNA from each sample was subjected to profiling on Human WG-DASL Assay with Human HT12 v4.0 BeadChips (Illumina Inc., San Diego, CA, USA) that allows the expression profiling of 29 377 probes from degraded RNA, such as that extracted from FFPE samples (Vallacchi *et al.*, 2014). Reverse transcription, oligo annealing, ligation, amplification, labeling, probe purification, hybridization, and chip's washing were performed following the manufacturer's instructions. Microarray chips were scanned with an Illumina BeadArray Reader. Primary data were extracted by

GENOME STUDIO software V.3 (Illumina Inc.), normalized by quantile algorithm, and exported without correcting for background or scale. All microarray data are MIAME compliant and the raw data were deposited into the NCBI's Gene Expression Omnibus (GEO) database (http://www.ncbi.nmlm.nih.gov/projects/geo/) with accession number GSE65021.

2.4. Statistical and bioinformatic analyses

Statistical analysis was performed using R Development Core Team, 2007 version 2.15, BioConductor (Available online: www.bioconductor.org) and the BRB-ArrayTool developed by Richard Simon and the BRB-ArrayTools Development Team (v4.2.0; National Cancer Institute, USA). Unsupervised tumor subtype identification was performed by ConsensusClusterPlus (Wilkerson and Hayes, 2010). Supervised class comparison was made to define the differentially expressed genes imposing a significance threshold of false discovery rate (FDR) < 1% and |log2 (fold change)| > 1 between WT and mutated *CTNNB1*-bearing samples. The probability of finding probe sets significant by chance (FDR at 0.01 level) was determined by the global test through 1000 permutations as computed by BRB tool using default parameters. Pathway analysis on 905 GO terms was performed using gene set enrichment analysis (GSEA). The degree of gene sets' enrichment in the WT and mutated DF was represented by a normalized enrichment score (NES) and NES with FDR < 0.05 and > |1.5| was considered statistically significant. Graphical representation of GSEA findings was provided by GOBubble plot function of GOplot R package (Wencke *et al.*, 2015), displaying information about the significance of the enrichment (−log10-adjusted *P*-value) and the z-score of each gene set. For comparison purposes, the gene list derived from 14 sporadic DF (not characterized for *CNTBB1* mutation) and five paired normal samples plus six solitary fibrous tumor specimens was analyzed (Colombo *et al.*, 2011). The list of 636 and 119 genes, up and down (see Table S2 in Colombo *et al.*, 2011) in DF, respectively, was imported in GSEA and used as custom gene sets and tested for enrichment in our gene expression dataset.

2.5. Nanostring nCounter System

The Nanostring nCounter System analysis was performed by Pharma Diagen (Padova, Italy) using the Human Inflammation panel (249 genes). Statistical analysis was conducted by comparing WT versus both mutated cases and then the mutation T41A versus S45F. Raw data from Nanostring platform were normalized by resorting to a two-step strategy using the R NanoStringNorm package (Waggott *et al.*, 2012). Firstly, by taking advantage of the negative and positive controls present in the Nanostring assay, a technical normalization was performed. A biological normalization was then implemented by using the housekeeping genes as endogenous controls. Subsequently, due to the limited sample size per group, we considered only that genes resulting expressed in all samples for the comparisons of interest. To analyze the normalized gene copies counts, a generalized linear model was implemented with a logarithmic link that takes into account overdispersion of the data (Agresti, 2007). Multiple testing adjustment, such as FDR correction (at 0.05 level), was used to manage the multiplicity problem. Statistical analyses were performed with R and SAS software (version 9.2.; SAS Institute Inc., Cary, NC, USA).

2.6. Immunohistochemical analysis

Immunohistochemistry was performed on 2-μm FFPE sections in an automated immunostainer (Autostainer Link48; Dako, Glostrup, Denmark) according to the manufacturer's instructions. The following antibodies were used: β-catenin 14 (1 : 1000; BD Transduction, South San Francisco, CA, USA), CD3 polyclonal (1 : 400; Dako), CD4 4B12 (1 : 300; Dako), CD8 C8/144B (1 : 20; Dako), CD20 L26 (1 : 400; Dako), CD21 1F8 (1 : 50; Dako), CD56 123C3 (1 : 400; Dako), CD68 KP1 (1 : 3000; Dako), CD163 10D6 (1 : 200; Novocastra, Newcastle, UK), FOXP3 259D/C7 (1 : 200; BD Pharmingen), PD-L1 SP142 (1 : 30; SPRING, Pleasanton, CA, USA), PD1 NAT105 (1 : 100; Biocare Medical, Pikenine, Concord, NC, USA), and EZH2 5246S (1 : 50; Cell Signaling, Leiden, Netherlands).

3. Results

3.1. *CTNNB1*-mutated and WT DFs have different thermodynamic stability and affinity for α-catenin

The N-terminal domain of β-catenin, which contains the residues T41 and S45, mediates protein degradation and interacts with α-catenin in the cell–cell adhesions mechanically coupling the actin cytoskeletons of adjacent cells (Jiang and Struhl, 1998; Pokutta *et al.*, 2014). In this scenario, we performed extensive MD simulations to investigate possible effects exerted by the two mutations T41A and S45F on the protein thermodynamic stability and on β-catenin/α-catenin dimer formation compared to β-catenin WT. To the purpose, the 3D model of the full-length β-catenin

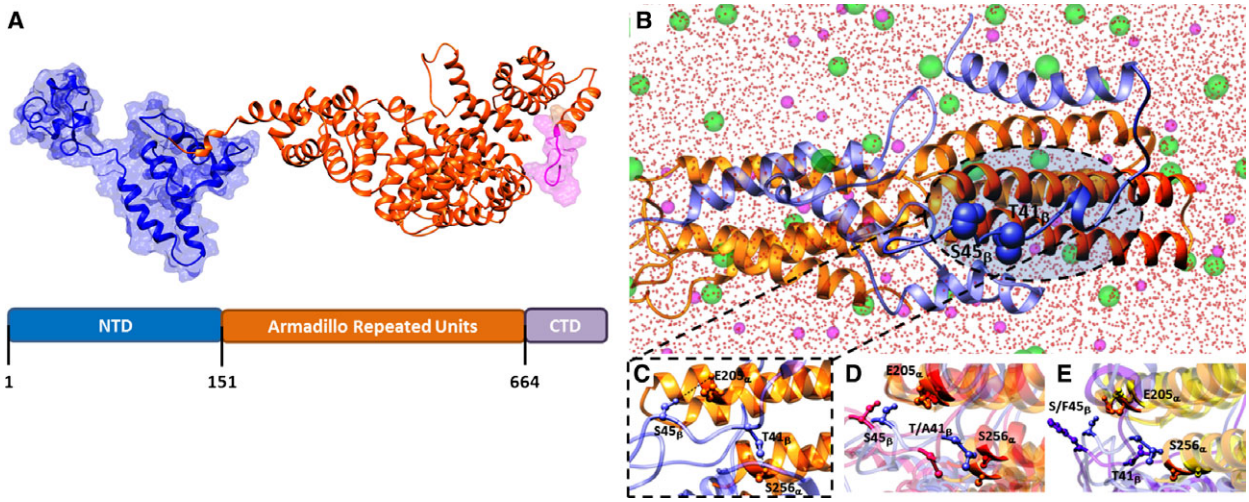

Fig. 1. Wild-type (WT) and mutated β-catenins have different thermodynamic stability and affinity for α-catenin. (A) Three-dimensional structure of the β-catenin WT protein. The different domains of β-catenin are shown in different colors (same for 3D model and diagram): N-terminal domain (NTD), blue; Armadillo repeated units, orange; C-terminal domain (CTD), purple. (B) Overall and (C) zoomed view of an equilibrated MD snapshot of the WT β-catenin/α-catenin complex. The proteins are visualized in ribbon style and colored as follows: α-catenin, cornflower blue; β-catenin, orange. Oxygen water atoms are represented as red spheres, while chlorine and sodium are depicted as green and purple spheres, respectively. (D) Superposition of MD-equilibrated snapshots of WT (cornflower blue) and the T41A (orange)-mutant β-catenin in complex with α-catenin. (E) Superposition of MD-equilibrated snapshots of WT (cornflower blue) and the S45F (purple)-mutant β-catenin in complex with α-catenin.

(Fig. 1A) was built starting from the available crystallographic structures and linking the missing loops previously modeled by computational techniques.

Computer-based simulations revealed that the thermodynamic stabilities (i.e., Gibbs free energy ΔG) of the two mutant T41A and S45F β-catenin isoforms are comparable ($\Delta G_{T41A} = -10\ 480.40 \pm 0.\ 22$ kcal·mol^{-1}, $\Delta G_{S45F} = -10\ 480.33 \pm 0.25$ kcal·mol^{-1}); rather, both mutant proteins showed a slightly increased stability compared to the WT counterpart, the T41A and S45F being more stable than the WT β-catenin by 1.33 kcal·mol^{-1} and 1.26 kcal·mol^{-1}, respectively.

Concerning β-catenin/α-catenin complex formation, computer simulations showed that protein/protein interface involves the N-terminal domain of β-catenin and two α-helices of α-catenin spanning residues P200-R229 and A234-Q259, respectively (Fig. 1B). We also noted that residues T41 and S45 of β-catenin play an active role in the complex formation, being involved in hydrogen bonds with the side chain of S256 and E205 α-catenin residues, respectively (Fig. 1C). The free energy of interaction (ΔG_{bind}) between α- and WT β-catenin is shown in the first row of Table S1. In addition, in the WT β-catenin, both hydrogen bonds connecting the two protein chains (through T41 on the β-chain and S256 on the α-chain, and S45 on the β-chain and E205 on the α-chain, respectively) were stable and characterized by an optimal average dynamic length (ADL) of 1.95 ± 0.03 and 1.96 ± 0.04 Å, respectively. The same simulation procedure applied to α-catenin in complex with the two mutant β-catenin chains showed that the affinity of both mutant isoforms for α-catenin is strongly reduced compared to the WT protein (by 2.74 and 2.87 kcal·mol^{-1}, respectively), ultimately resulting in the formation of a weaker complex (Table S1).

The presence of either missense substitutions (A and F at positions 41 and 45 of β-catenin, respectively) results in a plummet of the stabilizing interactions of the corresponding α-/β-catenin complexes. Indeed, the substitution of two polar residues, both featuring an –OH group available for hydrogen binding, with two residues devoid of such feature led to global conformational changes, which involve protein regions at a distal position from the mutant loci (Fig. 1D,E). As further indication of the detrimental effect exerted by the two mutations on the α-/β-catenin complex formation, we detected that the residual hydrogen bonds (i.e., the one between T41 on the β-catenin and S256 on α-catenin and between S45 on β-catenin and E205 on α-catenin, respectively) are longer, and hence, weaker, than in the case of the WT β-catenin/α-catenin complex ($ADL_{(T41\beta\text{-}S256\alpha)} = 2.15 \pm 0.04$ Å for the T41A-mutant and $ADL_{(S45\beta\text{-}E205\alpha)} = 2.14 \pm 0.06$ Å for the S45F-mutant complexes).

Overall, both mutant proteins were more stable than the WT β-catenin and formed a weaker complex with α-catenin due to longer hydrogen bonds.

3.2. *CTNNB1*-mutated and WT DFs have different gene expression profiles

We analyzed the gene expression profile of 33 primary surgical DFs entering our case material through DASL whole-genome microarrays, resulting in the detection of 20 284 probe sets corresponding to 14 664 unique genes. In order to explore the inherent gene expression patterns present in our dataset, consensus unsupervised clustering was applied and revealed the presence of two main clusters of DF samples (Fig. 2A upper panel), essentially reflecting *CTNNB1*-mutated cases (Cluster 1: 21/24 samples are mutated) and WT (Cluster 2: 6/9 samples are WT) ($P = 0.0047$ by χ^2, Fig. 2A lower panel). By supervised analysis and class comparison, we identified 382 differentially expressed probe sets (See Table S2 for details). The probability of finding 382 probes significant by chance if there were no real differences between the classes was 0.003, as determined by the global test. As depicted in Fig. 2B, 48 probes are upregulated in WT, while 334 are upregulated in *CTNNB1*-mutated DFs. The gene signatures derived from Colombo *et al*. (2011) comparing sporadic DFs ($n = 14$) and normal samples/solitary fibrous tumor specimens ($n = 11$) were applied to our dataset as custom gene sets in GSEA; this analysis identified in WT β-catenin cases a significant enrichment of genes present in normal tissues (Fig. 2C) and in mutated cases a significant enrichment of genes present in sporadic DFs (Fig. 2D).

To gain further insight into the biological pathways modulated by *CTNNB1* mutational status, GSEA analysis was performed. This analysis revealed six gene sets significantly enriched in *CTNNB1*-mutated DF as compared to WT DFs. The main difference between the WT and mutated tumors was associated with their contractile fiber status, being the WT DFs characterized by an enrichment of the genes sets 'Contractile Fiber', 'Structural Constituent Muscle', and 'Myofibril' (Fig. 3A). This is in line with the characteristics of DF in general where myofibroblasts are dismounted and collagen is increased.

3.3. T41A-mutated DFs have an upregulation of gene sets belonging to inflammatory status

No differentially expressed genes were observed when the two specific mutations T41A and S45F were compared. However, GSEA revealed four gene sets significantly enriched in *CTNNB1* T41A DFs when compared with S45F. The main difference between the two mutated tumor groups was associated with their inflammatory status, being the T41A DFs characterized by upregulation of genes of 'Inflammatory Response', 'Defense Response', 'Humoral Immune Response', and 'Antigen Binding' (Fig. 3B). In each of these four gene sets, the upregulated genes included mainly chemokine ligands and receptors and interleukins. This intriguing evidence suggested that the inflammation and immune response might play a role particularly in T41A cases.

3.4. T41A- and S45F-mutated DFs have different expression of inflammation-related genes

On the basis of the inflammation-related gene set enrichment found in T41A cases, we further explored by nanostring the expression of 249 inflammation-related biomarkers including chemokines, interleukins, growth factors, tool-like receptors.

Comparing both mutated (T41A + S45F) versus WT DFs, among the 139 biomarkers resulted to be expressed in all the 33 samples, only HMGN1 was found statistically significantly overexpressed in mutated DFs (adjusted FDR P-value = 0.009). This nucleosome-binding protein HMGN1 is a potent alarmin that promotes T cell-mediated antitumor immunity (Wei *et al*., 2014).

Further analysis comparing the two mutated groups demonstrated that 147 biomarkers were expressed in all the 24 samples; 16 of them were statistically significantly deregulated in the T41A compared with S45F cases (Table 2). In detail, 14 genes resulted to be overexpressed in T41A DFs (CREB1, MAPK3, CCL4, TLR2, HMGN1, MKNK1, MEF2A, IRF1, CD55, PPP1R12B, RAPGEF2, C2, PTGER2, TLR3) and TGF-β2 and TGF-β3 were downregulated.

Interestingly, some of these upregulated markers are known to be associated with antitumor immunity, such as HMGN1 (Wei *et al*., 2014); the transcription factor CREB1 that plays a key role in NF-kB inhibition, thereby limiting proinflammatory responses and enhancing host immune responses (Wen *et al*., 2010); IRF1 that contributes to tumor immune surveillance (Dou *et al*., 2014). Moreover, the lower levels of TGF-β2 and TGF-β3 we observed in T41A are intriguing due to the bifunctional role (pro- and anti-inflammatory) of these two cytokines recently described in immune system (Okamura *et al*., 2015).

Cumulatively, the main differences dictated by the RNA analyses were the augment of secreted proteins enhancing tumor immune response of T41A compared to S45F mutation.

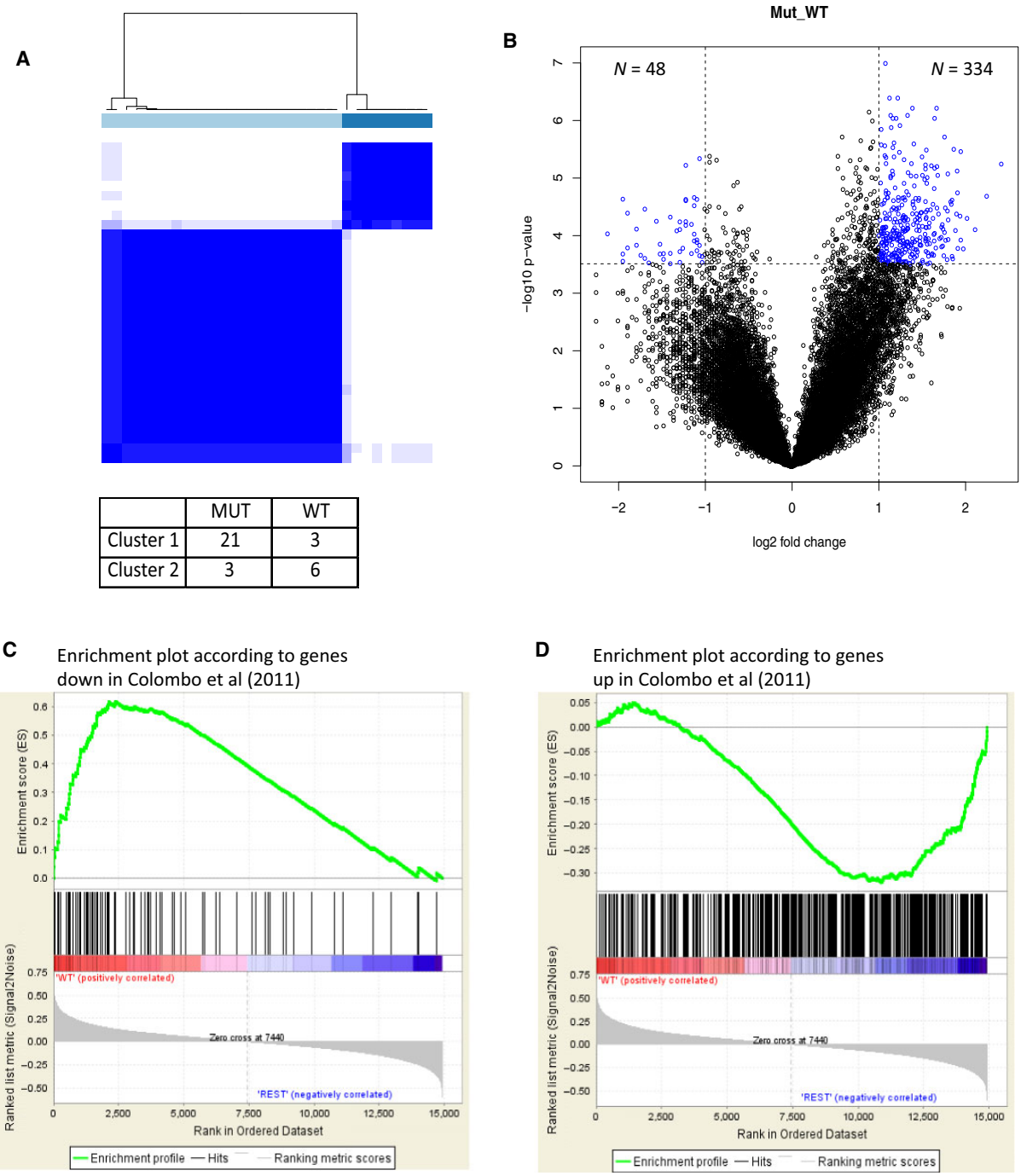

	MUT	WT
Cluster 1	21	3
Cluster 2	3	6

Fig. 2. Mutated and wild-type (WT) β-catenin desmoid-type fibromatosis (DFs) have different gene expression profiles. (A) Upper panel: consensus unsupervised clustering analysis of the gene expression of 33 DF samples (nine WT and 24 mutated); the heatmap depicts the consensus matrix imposing the presence of two clusters on the dataset. The values range from 0 (white, samples do not cluster together) to 1 (blue, samples showing high clustering affinity); lower panel: distribution of WT and mutated DF samples in the two clusters. (B) Volcano plot of $\log_2$ (fold changes) versus $-\log_{10}$ *P*-value. The volcano plot shows transcriptional differences between the two groups of samples identified by consensus unsupervised clustering analysis. The dashed lines denote the FDR < 0.01 cutoff. (C, D) The list of genes, down (119) and up (636), in sporadic DFs ($n = 14$) as compared to normal samples/solitary fibrous tumors ($n = 11$) (31), when used as custom gene set in GSEA, identified in WT *CTNNB1* cases (panel C) a significant enrichment of genes present in normal/solitary fibrous tissues, and in mutated *CTNNB1* cases (panel D) a significant enrichment of genes present in sporadic DF.

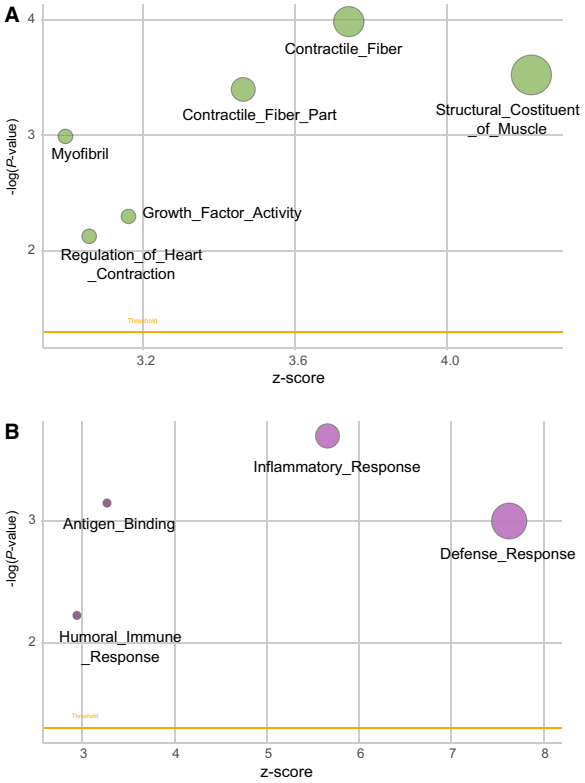

Fig. 3. Biological pathways modulated by *CTNNB1* mutational status. Bubble plot of gene sets significantly enriched in: (panel A) *CTNNB1*-mutated DF as compared to WT DF; (panel B) *CTNNB1* T41A DFs as compared to S45F. An overview of GSEA-enriched networks is depicted. The *x*-axis indicates the *z*-score for each term, while the *y*-axis is the negative logarithm of the adjusted *P*-value. The area of the displayed circles is proportional to the number of genes assigned to each term. DF, desmoid-type fibromatosis; WT, wild-type.

3.5. Host immunoscore system assessment in T41A- and S45F-mutated DFs

We made immunoscore assessment of the immunosystem-based biomarkers including CD3, CD4, CD8, FOXP3, CD20, CD56, CD21, CD163, and CD68. In terms of immunoprofile between the two types of mutations, no difference was observed. In all cases, the analysis revealed throughout the tumor proliferation a low number of T cells, $CD3^+$, and $CD8^+$ and of tumor-associated macrophages (TAM), $CD163^+$, and/or $CD68^+$, distributed around the vessels (Fig. 4A–C). In addition, a more consistent number of tumor-infiltrating lymphocytes (TILs), T cells, and/or TAMs were present at the boundaries, where the proliferation abutted the skeletal muscle, or in the area of entrapped muscle fibers which in all the cases exhibited marked regressive changes (Fig. 4D,E). No FOXP3-, CD4-, and CD56-immunolabeled cells were observed. In addition to T cells, $CD20^+$ B cells (Fig. 4F) were present in occasional small lymphoid aggregates that did not reach characteristics of tertiary lymphoid structures lacking CD21-decorated dendritic follicular cells and/or EZH2-positive (here applied as surrogate of activation) germinative centers (Fig. 4G) (Neyt *et al.*, 2012).

Despite the lack of a sizable number of EZH2 expressing T lymphocytes, we explored the expression of the costimulatory molecule PD-1 and its ligand PD-L1 in order to identify potential treatment window of the host immune system being, as expected, tumor cells always negative. The analysis, performed on nine cases, showed only few PD-1-decorated lymphocytes, mostly restricted to lymphoid aggregates (Fig. 4H), and no immunolabeled PD-L1 tumor-associated inflammatory cells (Fig. 4I).

Altogether, the host cellular immunocomponent was very poor, suggesting that the observed modulation of the secreted cytokines/chemokines was sustained by tumor cellular component other than the resident TILs and TAMs. By contrast, in all mutated and WT cases, all the tumor cells were β-catenin-immunodecorated.

Table 2. Nanostring analysis comparison between T41A- and S45F-mutated desmoid-type fibromatosis.

Gene	Fold change	*P*-value	Adjusted *P*-value
CREB1	1.3269	0.00001	0.0010
MAPK3	1.2038	0.00005	0.0037
CCL4	3.2859	0.00037	0.0168
TGFB2	0.5706	0.00055	0.0168
TLR2	1.4818	0.00066	0.0168
HMGN1	1.2573	0.00081	0.0168
MKNK1	1.2910	0.00087	0.0168
TGFB3	0.6707	0.00092	0.0168
MEF2	1.2359	0.00149	0.0242
IRF1	1.6080	0.0017	0.0242
CD55	1.6027	0.00183	0.0242
PPP1R12B	1.6331	0.00198	0.0242
RAPGEF2	1.1710	0.00312	0.0353
C2	1.6592	0.00472	0.0495
PTGER2	1.6147	0.00522	0.0498
TLR3	1.9329	0.00542	0.0498

4. Discussion

We started from the hypothesis that *CTNNB1* mutation types can influence the β-catenin stability and its affinity for α-catenin, besides the pattern of gene expression and consequently DF behavior.

The modeling results demonstrated that the presence of T41A or S45F mutation concurs in the stabilization of the mutated proteins compared to the WT, and in

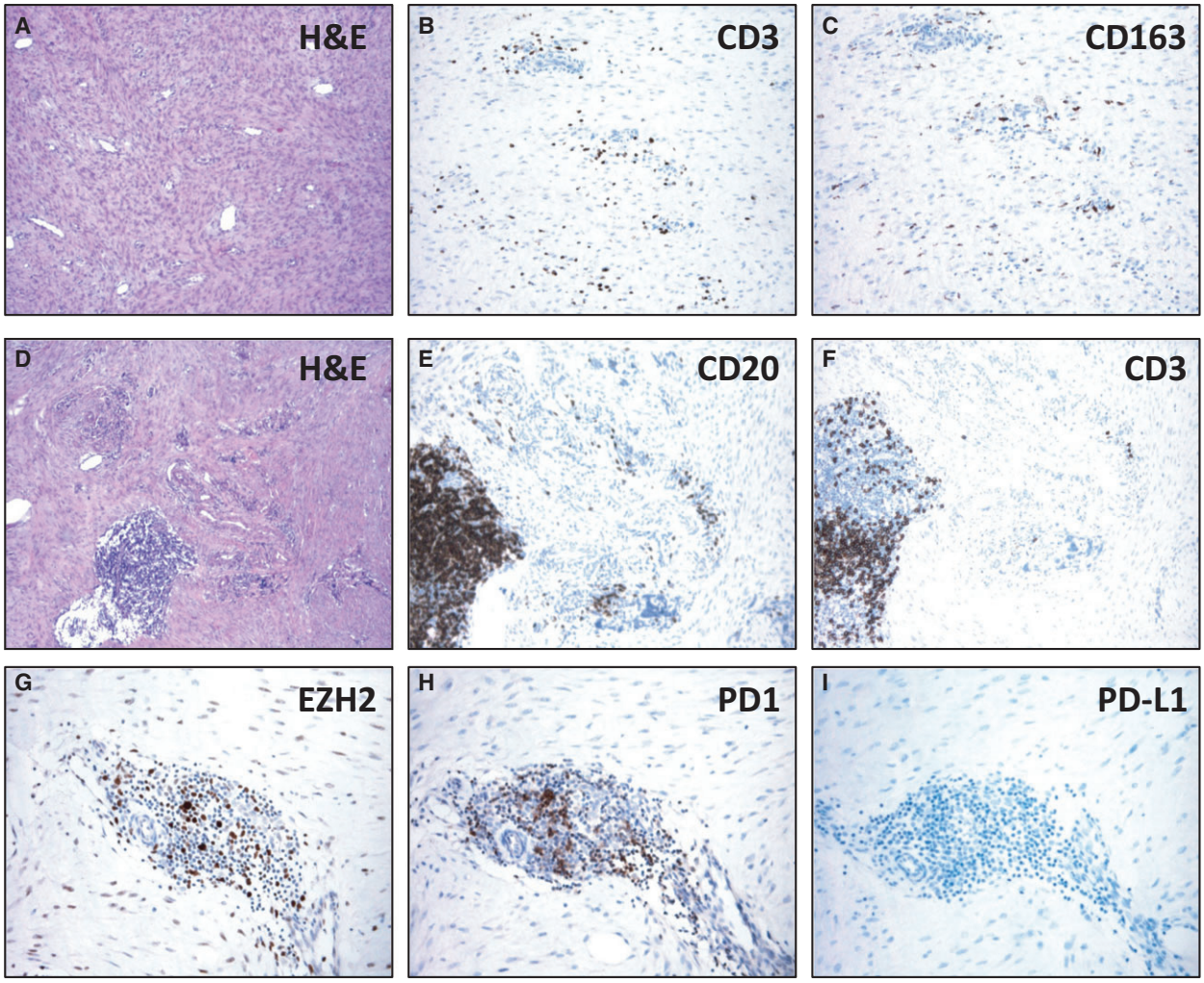

Fig. 4. T cells and tumor-associated macrophages (TAM) are rare in T41A- or S45F-mutated desmoid-type fibromatosis. In the tumor proliferation (A), a low number of $CD3^+$ T cells (B) and $CD163^+$ tumor-associated macrophages (C) were distributed around the vessels. In occasional small lymphoid aggregates (D), $CD20^+$ B cells (E), $CD3^+$ T cells (F), and $EZH2^+$ cells (G) were present. Few PD-1-decorated lymphocytes were restricted to lymphoid aggregates (H), and no immunolabeled PD-L1 tumor-associated inflammatory cell (I) was present.

the reduction in the affinity binding with α-catenin. The *in silico* results supported the assumption that both mutations shift the balance between membrane and cytoplasmic β-catenin toward a cytoplasmic/nuclear pool, as showed by the nuclear and cytoplasmic immunoreactivity of β-catenin in mutated DF (Signoroni *et al.*, 2007).

Next, we investigated by gene expression analysis the influence of the two mutations on β-catenin nuclear role as transcription factor. This analysis revealed that the group of T41A + S45F showed a distinct signature compared to WT DFs, suggesting that they are two distinct biological entities. Interestingly, the two different patterns of gene expression are in line with the clinical evidence that β-catenin WT DFs are associated with a better prognosis than mutated ones (van Broekhoven *et al.*, 2015; Colombo *et al.*, 2013; Dômont *et al.*, 2010).

Our profiling analysis is quite unique. Indeed, only a recent gene expression study compared mutated versus WT DFs, indicating that mutated DFs did not cluster separately and did not have a different clinical behavior from WT tumors (Crago *et al.*, 2015). However, the authors of this study included in the 'mutated' group also tumors lacking *CTNNB1* mutation but carrying other Wnt/β-catenin signaling alterations, such as *APC* mutations and/or loss. Thus, their results – rather than elucidating possible differences between *CTNNB1*-mutated and WT DFs – reflect the rarity of the 'wild-type' Wnt/β-catenin genotype. This prompted us to explore

APC status in our series by next-generation sequencing that revealed the absence of *APC* mutations in all but one *CTNNB1* WT case (data not shown).

The other gene expression analyses on DFs reported in the literature are not comparable with our study because, regardless of tumor *CTNNB1* mutational status, they compared DFs with nodular fasciitis, normal tissues, and/or solitary fibrous tumors in order to find specific gene signatures associated with DF biology or outcome (Bacac *et al.*, 2006; Colombo *et al.*, 2011; Denys *et al.*, 2004; Salas *et al.*, 2010; Skubitz and Skubitz, 2004). However, it should be mentioned that one of these studies comparing DFs with normal tissues identified two distinct subgroups of DFs on the basis of gene expression profiles that paralleled different clinical outcomes (Skubitz and Skubitz, 2004). Interestingly, the subsequent sequencing of the same samples revealed that these two subclusters showed different β-catenin mutation distribution (Misemer *et al.*, 2014), even if the exiguous number of analyzed cases did not allow drawing any definitive conclusion.

When the gene signatures previously obtained comparing sporadic DFs and normal/solitary fibrous samples were applied to our dataset as custom gene sets in GSEA, we found a significant enrichment of genes described in normal tissues in the group of WT β-catenin DFs, and an enrichment of genes present in sporadic DFs in the mutated cases (Colombo *et al.*, 2011). This evidence suggests that WT DFs share molecular characteristics with normal tissue that may explain their better prognosis than mutated DFs.

No differently expressed genes were observed when the two specific mutations T41A and S45F were compared, supporting that the two specific mutations dictate a similar transcriptional activity of the two corresponding mutant β-catenin proteins. However, when the comparison between T41A and S45F was made using gene ontology enrichment analysis, a difference in specific pathways belonging to 'Inflammatory Response', 'Defense Response', 'Humoral Immune Response', and 'Antigen Binding' emerged. As DFs have unpredictable clinical course, an equilibrium between host and disease may be crucial. To further investigate a possible role of immune system/inflammation in DFs, the expression of human inflammation-related biomarkers was assessed by Nanostring. According to gene ontology enrichment analysis, the comparison between the two mutated DFs revealed 16 genes statistically significant up- or down-regulated in T41A compared with S45F DFs. Due to the known relationship between oncogene activation and inflammation according to which oncogenes can also regulate the inflammatory milieu in tumors (Dibra *et al.*, 2014), we can speculate that by activating specific pro- and anti-inflammatory mediators, the two *CTNNB1* mutations may produce a different inflammatory milieu that can have different impact on DF behavior. Coherently, T41A cases, generally associated with better prognosis after surgery, showed overexpression of anti-inflammatory markers associated with antitumor immunity, such as CREB1, HMGN1, MKNK1 and IRF1, as well as lower levels of TGF-β3 and TGF-β2 associated with proinflammatory activities. We believe that these biomarkers were mainly derived from tumor cells because throughout all tumor proliferations, from which RNA has been extracted for gene expression, only a low number of TILs and TAMs were observed and a more consistent number of TILs, T cells, and/or TAMs were all restricted to the boundaries of DFs, where the proliferation abutted the skeletal muscle or in the area of entrapped muscle fibers. This peculiar inflammatory microenvironment is in line with the hypothesis that β-catenin signaling activation, from which DFs depend, results in T-cell exclusion favoring the immune evasion. Indeed, by inhibiting T-cell activation, β-catenin activation is one of the mechanisms that melanoma can use to evade antitumor immunity (Spranger *et al.*, 2015). Here, the PD1/PD-L1 profile of DFs fell into the group defined 'the noninflamed tumor type', which is closely associated with the EMT/STEM-like type controlled by oncogenic and epigenetic pathways including β-catenin, and is predictive of no clinical response of DFs to immune-based therapies (Zou *et al.*, 2016). Rather, the pharmacological inhibition of β-catenin activity for tumor therapy has come into the focus of drug development (Käfer *et al.*, 2016). Moreover, the difference in the inflammatory milieu between the two mutated forms T41A and S45F deserves further study as it can be useful in guiding future tailored therapies.

In conclusion, our study demonstrated that DFs carrying T41A or S45F mutations and WT β-catenin are two distinct molecular subgroups with regard to β-catenin stability, α-catenin affinity, and gene expression profiling. Particularly, WT DFs showed an expression profile more similar to normal tissues, in keeping with their better prognosis. Moreover, we provided evidence that a different inflammation signature characterized S45F- and T41A-mutated cases, suggesting a specific inflammation setting mediated by the type of β-catenin mutation. Finally, all mutated cases showed a low number of TIL and TAM cells and a low or absent expression of PD-1 and PD-L1, consistent with β-catenin activation insensitive to checkpoint blockade. Considering the limitations of the study (small sample size, single-center experience), further studies are needed to confirm our data.

Acknowledgements

This work has been financially supported by Ministero della Salute, Ricerca Finalizzata 2009 (RF-2009-1511297, AG). The financial support from AIRC (IG 17413, Sabrina Pricl; MFAG 11758, Chiara Colombo), DTRF (Chiara Colombo), and the Research Fund of the University of Trieste (FRA 2016; Erik Laurini) is also gratefully acknowledged.

Author contributions

CC, FP, Sabrina Pricl, and Silvana Pilotti involved in conception and design; CC, AB, NP, LD, EL, MF, and SB acquired data; FP, Sabrina Pricl, SC, and PV analyzed and interpreted the data; AG, Silvana Pilotti, SS, MF, and EP participated in revising the article. All the authors gave final approval of the version to be submitted.

References

Agresti A. (2007) *Introduction to Categorical Data Analysis*, 2nd edn. John Wiley & Sons, Inc., Hoboken, NJ.

Bacac M, Migliavacca E, Stehle JC, McKee T, Delorenzi M, Coindre JM, Guillou L and Stamenkovic I (2006) A gene expression signature that distinguishes desmoid tumours from nodular fasciitis. *J Pathol* **208**, 543–553.

Bonvalot S, Eldweny H, Haddad V, Rimareix F, Missenard G, Oberlin O, Vanel D, Terrier P, Blay JY, Le Cesne A *et al.* (2008) Extra-abdominal primary fibromatosis: aggressive management could be avoided in a subgroup of patients. *Eur J Surg Oncol* **34**, 462–468.

Bozzi F, Conca E, Laurini E, Posocco P, Lo Sardo A, Jocollè G, Sanfilippo R, Gronchi A, Perrone F, Tamborini E *et al.* (2013) In vitro and in silico studies of MDM2/MDMX isoforms predict Nutlin-3A sensitivity in well/de-differentiated liposarcomas. *Lab Invest* **93**, 1232–1240.

van Broekhoven DL, Verhoef C, Grünhagen DJ, van Gorp JM, den Bakker MA, Hinrichs JW, de Voijs CM and van Dalen T (2015) Prognostic value of CTNNB1 gene mutation in primary sporadic aggressive fibromatosis. *Ann Surg Oncol* **22**, 1464–1470.

Colombo C, Creighton CJ, Ghadimi MP, Bolshakov S, Warneke CL, Zhang Y, Lusby K, Zhu S, Lazar AJ, West RB *et al.* (2011) Increased midkine expression correlates with desmoid tumour recurrence: a potential biomarker and therapeutic target. *J Pathol* **225**, 574–582.

Colombo C, Miceli R, Lazar AJ, Perrone F, Pollock RE, Le Cesne A, Hartgrink HH, Cleton-Jansen AM, Domont J, Bovée JV *et al.* (2013) CTNNB1 45F mutation is a molecular prognosticator of increased postoperative primary desmoid tumor recurrence: an independent, multicenter validation study. *Cancer* **119**, 3696–3702.

Crago AM, Chmielecki J, Rosenberg M, O'Connor R, Byrne C, Wilder FG, Thorn K, Agius P, Kuk D, Socci ND *et al.* (2015) Near universal detection of alterations in CTNNB1 and Wnt pathway regulators in desmoid-type fibromatosis by whole-exome sequencing and genomic analysis. *Genes Chromosom Cancer* **54**, 606–615.

Denys H, Jadidizadeh A, Amini Nik S, Van Dam K, Aerts S, Alman BA, Cassiman JJ and Tejpar S (2004) Identification of IGFBP-6 as a significantly downregulated gene by beta-catenin in desmoid tumors. *Oncogene* **23**, 654–664.

Dibra D, Mishra L and Li S (2014) Molecular mechanisms of oncogene-induced inflammation and inflammation-sustained oncogene activation in gastrointestinal tumors: an under-appreciated symbiotic relationship. *Biochim Biophys Acta* **1846**, 152–160.

Dileo P, Pricl S, Tamborini E, Negri T, Stacchiotti S, Gronchi A, Posocco P, Laurini E, Coco P, Fumagalli E *et al.* (2011) Imatinib response in two GIST patients carrying two hitherto functionally uncharacterized PDGFRA mutations: an imaging, biochemical and molecular modeling study. *Int J Cancer* **128**, 983–990.

Dômont J, Salas S, Lacroix L, Brouste V, Saulnier P, Terrier P, Ranchère D, Neuville A, Leroux A, Guillou L *et al.* (2010) High frequency of beta-catenin heterozygous mutations in extra-abdominal fibromatosis: a potential molecular tool for disease management. *Br J Cancer* **102**, 1032–1036.

Dou L, Liang HF, Geller DA, Chen YF and Chen XP (2014) The regulation role of interferon regulatory factor-1 gene and clinical relevance. *Hum Immunol* **75**, 1110–1114.

Ferrone M, Perrone F, Tamborini E, Paneni MS, Fermeglia M, Suardi S, Pastore E, Delia D, Pierotti MA, Pricl S *et al.* (2006) Functional analysis and molecular modeling show a preserved wild-type activity of p53(C238Y). *Mol Cancer Ther* **5**, 1467–1473.

Fiore M, Rimareix F, Mariani L, Domont J, Collini P, Le Péchoux C, Casali PG, Le Cesne A, Gronchi A and Bonvalot S (2009) Desmoid-type fibromatosis: a front-line conservative approach to select patients for surgical treatment. *Ann Surg Oncol* **16**, 2587–2593.

Gibbons DL, Pricl S, Posocco P, Laurini E, Fermeglia M, Sun H, Talpaz M, Donato N and Quintás-Cardama A (2014) Molecular dynamics reveal BCR-ABL1 polymutants as a unique mechanism of resistance to PAN-BCR-ABL1 kinase inhibitor therapy. *Proc Natl Acad Sci U S A* **111**, 3550–3555.

Hamada S, Urakawa H, Kozawa E, Arai E, Ikuta K, Sakai T, Ishiguro N and Nishida Y (2016)

Characteristics of cultured desmoid cells with different CTNNB1 mutation status. *Cancer Med* **5**, 352–360.

Jiang J and Struhl G (1998) Regulation of the Hedgehog and Wingless signalling pathways by the F-box/WD40-repeat protein Slimb. *Nature* **391**, 493–496.

Käfer R, Usanova S, Montermann E, Loquai C, Reske-Kunz AB and Bros M (2016) Inhibitors of β-catenin affect the immuno-phenotype and functions of dendritic cells in an inhibitor-specific manner. *Int Immunopharmacol* **32**, 118–124.

Kasper B, Baumgarten C, Bonvalot S, Haas R, Haller F, Hohenberger P, Moreau G, van der Graaf WT, Gronchi A; Desmoid Working Group (2015) Management of sporadic desmoid-type fibromatosis: a European consensus approach based on patients' and professionals' expertise – a sarcoma patients EuroNet and European Organisation for Research and Treatment of Cancer/Soft Tissue and Bone Sarcoma Group initiative. *Eur J Cancer* **51**, 127–136.

Kasper B, Gruenwald V, Reichardt P, Bauer S, Hohenberger P and Haller F (2016) Correlation of CTNNB1 mutation status with progression arrest rate in RECIST progressive desmoid-type fibromatosis treated with imatinib: translational research results from a Phase 2 Study of the German Interdisciplinary Sarcoma Group (GISG-01). *Ann Surg Oncol* **23**, 1924–1927.

Kundu JK, Choi KY and Surh YJ (2006) β-Catenin-mediated signaling: a novel molecular target for chemoprevention with anti-inflammatory substances. *Biochim Biophys Acta* **1765**, 14–24.

Laurini E, Col VD, Mamolo MG, Zampieri D, Posocco P, Fermeglia M, Vio L and Pricl S (2011) Homology model and docking-based virtual screening for ligands of the σ1 receptor. *ACS Med Chem Lett* **2**, 834–839.

Lazar AJ, Tuvin D, Hajibashi S, Habeeb S, Bolshakov S, Mayordomo-Aranda E, Warneke CL, Lopez-Terrada D, Pollock RE and Lev D (2008) Specific mutations in the beta-catenin gene (CTNNB1) correlate with local recurrence in sporadic desmoid tumors. *Am J Pathol* **173**, 1518–1527.

Misemer BS, Skubitz AP, Carlos Manivel J, Schmechel SC, Cheng EY, Henriksen JC, Koopmeiners JS, Corless CL and Skubitz KM (2014) Expression of FAP, ADAM12, WISP1, and SOX11 is heterogeneous in aggressive fibromatosis and spatially relates to the histologic features of tumor activity. *Cancer Med* **3**, 81–90.

Mittempergher L, de Ronde JJ, Nieuwland M, Kerkhoven RM, Simon I, Rutgers EJ, Wessels LF and Van't Veer LJ (2011) Gene expression profiles from formalin fixed paraffin embedded breast cancer tissue are largely comparable to fresh frozen matched tissue. *PLoS One* **6**, 1467–1473.

Morgan A, Gandin I, Belcaro C, Palumbo P, Palumbo O, Biamino E, Dal Col V, Laurini E, Pricl S, Bosco P *et al.* (2015) Target sequencing approach intended to discover new mutations in non-syndromic intellectual disability. *Mutat Res* **781**, 32–36.

Mullen JT, DeLaney TF, Rosenberg AE, Le L, Iafrate AJ, Kobayashi W, Szymonifka J, Yeap BY, Chen YL, Harmon DC *et al.* (2013) β-Catenin mutation status and outcomes in sporadic desmoid tumors. *Oncologist* **18**, 1043–1049.

Negri T, Pavan GM, Virdis E, Greco A, Fermeglia M, Sandri M, Pricl S, Pierotti MA, Pilotti S and Tamborini E (2009) T670X KIT mutations in gastrointestinal stromal tumors: making sense of missense. *J Natl Cancer Inst* **101**, 194–204.

Neyt K, Perros F, GeurtsvanKessel CH, Hammad H and Lambrecht BN (2012) Tertiary lymphoid organs in infection and autoimmunity. *Trends Immunol* **33**, 297–305.

Nishida Y, Tsukushi S, Urakawa H, Hamada S, Kozawa E, Ikuta K, Ando Y and Ishiguro N (2015) Low-dose chemotherapy with methotrexate and vinblastine for patients with desmoid tumors: relationship to CTNNB1 mutation status. *Int J Clin Oncol* **20**, 1211–1217.

Okamura T, Morita K, Iwasaki Y, Inoue M, Komai T, Fujio K and Yamamoto K (2015) Role of TGF-β3 in the regulation of immune responses. *Clin Exp Rheumatol* **33**, S63–S69.

Pierotti MA, Negri T, Tamborini E, Perrone F, Pricl S and Pilotti S (2010) Targeted therapies: the rare cancer paradigm. *Mol Oncol* **4**, 19–37.

Pierotti MA, Tamborini E, Negri T, Pricl S and Pilotti S (2011) Targeted therapy in GIST: in silico modeling for prediction of resistance. *Nat Rev Clin Oncol* **8**, 161–170.

Pokutta S, Choi HJ, Ahlsen G, Hansen SD, Weis WI (2014) Structural and thermodynamic characterization of cadherin β-catenin α-catenin complex formation. *J Biol Chem* **289**, 13589–13601.

Pricl S, Cortelazzi B, Dal Col V, Marson D, Laurini E, Fermeglia M, Licitra L, Pilotti S, Bossi P and Perrone F (2015) Smoothened (SMO) receptor mutations dictate resistance to vismodegib in basal cell carcinoma. *Mol Oncol* **9**, 389–397.

Ravo M, Mutarelli M, Ferraro L, Grober OM, Paris O, Tarallo R, Vigilante A, Cimino D, De Bortoli M, Nola E *et al.* (2008) Quantitative expression profiling of highly degraded RNA from formalin-fixed, paraffin-embedded breast tumor biopsies by oligonucleotide microarrays. *Lab Invest* **88**, 430–440.

Romero S, Szafranska J, Cabrera E, Gonzalez A, Peiró A, Llauger J, Ortega L, Bague S, Canet B, Espinosa I *et al.* (2012) Role of tumor-associated macrophages and angiogenesis in desmoid-type fibromatosis. *Virchows Arch* **461**, 117–122.

Salas S, Chibon F, Noguchi T, Terrier P, Ranchere-Vince D, Lagarde P, Benard J, Forget S, Blanchard C, Dômont J *et al.* (2010) Molecular characterization by

array comparative genomic hybridization and DNA sequencing of 194 desmoid tumors. *Genes Chromosom Cancer* **49**, 560–568.

Signoroni S, Frattini M, Negri T, Pastore E, Tamborini E, Casieri P, Orsenigo M, Da Riva L, Radice P, Sala P *et al*. (2007) Cyclooxygenase-2 and platelet-derived growth factor receptors as potential targets in treating aggressive fibromatosis. *Clin Cancer Res* **13**, 5034–5040.

Skubitz KM and Skubitz AP (2004) Gene expression in aggressive fibromatosis. *J Lab Clin Med* **143**, 89–98.

Spranger S, Bao R and Gajewski TF (2015) Melanoma-intrinsic catenin signaling prevents anti-tumour immunity. *Nature* **523**, 231–235.

Vallacchi V, Vergani E, Camisaschi C, Deho P, Cabras AD, Sensi M, De Cecco L, Bassani N, Ambrogi F, Carbone A *et al*. (2014) Transcriptional profiling of melanoma sentinel nodes identify patients with poor outcome and reveal an association of CD30(+) T lymphocytes with progression. *Cancer Res* **74**, 130–140.

Waggott D, Chu K, Yin S, Wouters BG, Liu F and Boutros PC (2012) NanoStringNorm: an extensible R package for the pre-processing of NanoString mRNA and miRNA data. *Bioinformatics* **28**, 1546–1548.

Wei F, Yang D, Tewary P, Li Y, Li S, Chen X, Howard OM, Bustin M, Oppenheim JJ (2014) Alarmin HMGN1 contributes to antitumor immunity and is a potent immunoadjuvant. *Cancer Res* **74**, 5989–5998.

Wen AY, Sakamoto KM and Miller LS (2010) The role of the transcription factor CREB in immune function. *J Immunol* **185**, 6413–6419.

Wencke W, Sánchez-Cabo F and Ricote M (2015) GOplot: an R package for visually combining expression data with functional analysis. *Bioinformatics* **31**, 2912–2914.

Wilkerson MD and Hayes DN (2010) ConsensusClusterPlus: a class discovery tool with confidence assessments and item tracking. *Bioinformatics* **26**, 1572–1573.

Zou W, Wolchok JD, Chen L (2016) PD-L1 (B7-H1) and PD-1 pathway blockade for cancer therapy: mechanisms, response biomarkers, and combinations. *Sci Transl Med* **8**, 328rv4.

Supporting information

Additional Supporting Information may be found online in the supporting information tab for this article:

Table S1. Binding free energies (ΔG_{bind}) and binding free energy differences ($\Delta\Delta G_{bind}$) for the WT, T41A and S45F β-catenin in complex with α-catenin.

Table S2. List of the 382 genes differentially expressed between mutated- and wt-DT patients.

Data S1. Computational details.

Supplementary Table 1. Binding free energies (ΔG_{bind}) and binding free energy differences ($\Delta\Delta G_{bind}$) for the WT, T41A and S45F β-catenin in complex with α-catenin.

	ΔG_{bind} (kcal/mol)	$\Delta\Delta G_{bind}$ (kcal/mol)
WT	-13.15 ± 0.26	-
T41A	-10.41 ± 0.28	-2.74
S45F	-10.28 ± 0.28	-2.87

According to its definition ($\Delta\Delta G_{bind}=\Delta G_{bind(WT)}-\Delta G_{bind(MUT)}$), negative values of $\Delta\Delta G_{bind}$ indicate that the considered amino acid substitution at a given position of β-catenin is unfavorable in terms of interaction with α-catenin.

Supplementary Table 2: List of the 382 genes differentially expressed between mutated- and wt-D

EntrezID	Clone	GB accession number	Gene symbol	Parametric p-value	FDR
Unique id	GB acc	Gene symbol	EntrezID	Parametric p-valu	FDR
ILMN_1804562	NM_001859	SLC31A1	1317	0,0000001	0,00166
ILMN_1722680	NM_032160	DSEL	92126	0,0000004	0,00166
ILMN_2192032	NM_003135	SRP19	6728	0,0000004	0,00166
ILMN_1815346	NM_174926	TMEM136	219902	0,0000006	0,00166
ILMN_1725175	NM_005253	FOSL2	2355	0,0000006	0,00166
ILMN_2124471	NM_078483	SLC36A1	206358	0,0000008	0,00166
ILMN_1722900	NM_001416	EIF4A1	1973	0,0000008	0,00166
ILMN_1766221	NM_001497	B4GALT1	2683	0,0000009	0,00166
ILMN_2128087	NM_001011713	NAT12	122830	0,0000009	0,00166
ILMN_3245611	NM_001098800	MAGED4	728239	0,0000009	0,00166
ILMN_1656915	NM_015310	PSD3	23362	0,0000012	0,00187
ILMN_1721901	NM_003798	CTNNAL1	8727	0,0000013	0,00188
ILMN_1708743	NM_022908	NT5DC2	64943	0,0000014	0,00189
ILMN_1789136	NM_001018108	SERF2	10169	0,0000019	0,00227
ILMN_1657547	NM_030771	CCDC34	91057	0,0000024	0,00232
ILMN_2328327	NM_134269	SMTN	6525	0,0000025	0,00232
ILMN_2325028	NM_001007022	ODF2L	57489	0,0000026	0,00232
ILMN_1686981	NM_018837	SULF2	55959	0,0000027	0,00232
ILMN_2268618	NM_198513	PHF20L1	51105	0,0000029	0,00232
ILMN_1734138	NM_014760	TATDN2	9797	0,0000031	0,00232
ILMN_1651343	NM_001004439	ITGA11	22801	0,0000032	0,00232
ILMN_1792710	NM_001348	DAPK3	1613	0,0000034	0,00237
ILMN_3226505	NM_078629	MSL3	10943	0,0000035	0,00237
ILMN_2348512	NM_001040653	ZXDC	79364	0,000004	0,00242
ILMN_2386530	NM_213725	RPLP1	6176	0,0000042	0,00242
ILMN_1693431	NM_153218	C13orf31	144811	0,0000042	0,00242
ILMN_2363106	NM_001077352	RBM23	55147	0,0000043	0,00242
ILMN_1715181	NM_015683	ARRDC2	27106	0,0000045	0,00242
ILMN_3249110	NM_030809	CSRNP2	81566	0,0000047	0,00242
ILMN_1658928	NM_005273	GNB2	2783	0,0000055	0,0025
ILMN_2405642	NM_024887	DHDDS	79947	0,0000055	0,0025
ILMN_1740559	NM_000131	F7	2155	0,0000056	0,0025
ILMN_1755134	NM_002154	HSPA4	3308	0,0000058	0,0025
ILMN_1652333	NM_024619	FN3KRP	79672	0,0000059	0,0025
ILMN_3310321	NR_003231	SNORD113-3	767563	0,000006	0,0025
ILMN_1760563	NM_080686	BAT2	7916	0,0000062	0,0025
ILMN_2406873	NM_175609	ARFGAP1	55738	0,0000066	0,0025
ILMN_3307705	NM_178276	SERINC5	256987	0,0000068	0,0025
ILMN_2296644	NM_018921	PCDHGA9	56107	0,0000074	0,00259
ILMN_2367020	NM_014302	SEC61G	23480	0,0000074	0,00259
ILMN_1710622	NM_144565	DUOXA1	90527	0,0000079	0,00272
ILMN_3309854	NR_003237	SNORD113-9	767569	0,0000083	0,00275
ILMN_3245764	NR_002972	SNORA39	677821	0,0000085	0,00275
ILMN_2083559	NM_014855	KIAA0415	9907	0,0000088	0,00275
ILMN_1652907	NM_001253	CDC5L	988	0,0000088	0,00275

ILMN_1804945	NM_022103	ZNF667	63934	0,000009	0,00275
ILMN_1736856	NM_017990	PDPR	55066	0,0000091	0,00275
ILMN_3236102	NR_002755	RNU5D	26830	0,0000091	0,00275
ILMN_3251616	NM_152519	C2orf67	151050	0,0000096	0,00276
ILMN_1697418	NM_001082576	RBM9	23543	0,0000097	0,00276
ILMN_1796341	NM_001010983	GLT8D1	55830	0,0000104	0,00285
ILMN_1678541	NM_139321	ATRN	8455	0,0000119	0,00307
ILMN_1694367	NR_001285	SNORD35B	84546	0,0000121	0,00307
ILMN_2178775	NM_152279	ZNF585B	92285	0,0000121	0,00307
ILMN_1770244	NM_006807	CBX1	10951	0,0000134	0,00331
ILMN_2099249	NM_006980	MTERF	7978	0,0000145	0,00354
ILMN_1682717	NM_003897	IER3	8870	0,0000149	0,0036
ILMN_2411963	NM_184234	RBM39	9584	0,0000164	0,00378
ILMN_1716382	NM_207376	LOC387882	387882	0,0000169	0,00381
ILMN_1757378	NM_000445	PLEC1	5339	0,0000177	0,0039
ILMN_1768470	NM_182917	EIF4G1	1981	0,0000179	0,0039
ILMN_2160388	NM_000986	RPL24	6152	0,0000182	0,00393
ILMN_1752285	NM_000968	RPL4	6124	0,0000193	0,00399
ILMN_3230572	NR_024205	NCRNA00152	112597	0,0000203	0,00402
ILMN_3309036	NR_003204	SNORD114-11	767589	0,0000213	0,00402
ILMN_1666380	NM_178007	STARD13	90627	0,0000213	0,00402
ILMN_1767351	NM_001011645	AR	367	0,0000214	0,00402
ILMN_3251317	NM_007033	RER1	11079	0,0000214	0,00402
ILMN_1711048	NM_003443	ZBTB17	7709	0,0000215	0,00402
ILMN_1794349	NM_005108	XYLB	9942	0,0000219	0,00402
ILMN_1693244	NM_001003801	SMARCD3	6604	0,0000221	0,00402
ILMN_2412564	NM_007362	NCBP2	22916	0,0000221	0,00402
ILMN_2073289	NM_014751	MTSS1	9788	0,0000228	0,00402
ILMN_1694325	NM_002501	NFIX	4784	0,000023	0,00402
ILMN_1810852	NM_002293	LAMC1	3915	0,0000231	0,00402
ILMN_2346358	NM_138923	TAF1	6872	0,0000236	0,00402
ILMN_1676305	NM_153831	PTK2	5747	0,0000237	0,00402
ILMN_1695604	NM_173674	DCBLD1	285761	0,0000237	0,00402
ILMN_2383077	NM_001077516	SLC39A7	7922	0,000024	0,00402
ILMN_2344182	NM_032813	TMTC4	84899	0,000024	0,00402
ILMN_1797731	NM_022349	MS4A6A	64231	0,0000242	0,00402
ILMN_1689004	NM_016639	TNFRSF12A	51330	0,0000242	0,00402
ILMN_2148785	NM_002053	GBP1	2633	0,0000251	0,00412
ILMN_1662483	NM_021036	SMA5	11042	0,0000253	0,00412
ILMN_1772614	NM_207040	TCF12	6938	0,0000254	0,00412
ILMN_2112493	NM_004394	DAP	1611	0,0000269	0,00426
ILMN_2246256	NM_005054	RGPD5	84220	0,000028	0,00435
ILMN_1687023	NM_001080383	GJC1	10052	0,000028	0,00435
ILMN_1699473	NM_021174	KIAA1967	57805	0,0000281	0,00435
ILMN_1750246	NM_014950	ZBTB1	22890	0,0000283	0,00435
ILMN_2363439	NM_002958	RYK	6259	0,0000287	0,00436
ILMN_2106449	NM_024613	PLEKHF2	79666	0,0000296	0,00441
ILMN_2063687	NM_020787	ZNF624	57547	0,0000321	0,00447
ILMN_1735958	NM_018396	METTL2B	55798	0,0000324	0,00447
ILMN_2082324	NM_152313	SLC36A4	120103	0,0000325	0,00447

ILMN_1736101	NM_147193	GLIS1	148979	0,0000325	0,00447
ILMN_1716651	NM_001024630	RUNX2	860	0,0000325	0,00447
ILMN_1706590	NM_005934	MLLT1	4298	0,0000329	0,00448
ILMN_1669696	NM_175872	ZNF792	126375	0,0000337	0,00454
ILMN_2302757	NM_003890	FCGBP	8857	0,0000339	0,00454
ILMN_1806946	NM_001076683	UBTF	7343	0,0000347	0,00457
ILMN_2180997	NM_001003795	GTF2IRD2B	389524	0,0000347	0,00457
ILMN_1700248	NM_198285	WDR86	349136	0,0000349	0,00457
ILMN_1766593	NM_020901	PHRF1	57661	0,0000354	0,0046
ILMN_2153916	NM_021979	HSPA2	3306	0,0000366	0,0047
ILMN_1706304	NM_017629	EIF2C4	192670	0,0000381	0,00483
ILMN_3247882	NM_024066	ERI3	79033	0,0000388	0,00483
ILMN_1756086	NM_023015	INTS3	65123	0,0000393	0,00483
ILMN_2189037	NM_018338	WDR52	55779	0,0000398	0,00483
ILMN_1660808	NM_021197	WFDC1	58189	0,0000399	0,00483
ILMN_1672331	NM_015093	MAP3K7IP2	23118	0,0000406	0,00483
ILMN_3247494	NR_002994	SNORA36B	677818	0,0000409	0,00483
ILMN_1726410	NM_000485	APRT	353	0,000041	0,00483
ILMN_1706817	NM_014445	SERP1	27230	0,0000412	0,00483
ILMN_1695468	NM_182692	SRPK2	6733	0,0000413	0,00483
ILMN_1677384	NM_198719	PTGER3	5733	0,0000413	0,00483
ILMN_1688381	NM_004459	BPTF	2186	0,0000414	0,00483
ILMN_1682034	NM_012259	HEY2	23493	0,000044	0,00507
ILMN_1796669	NM_000021	PSEN1	5663	0,0000445	0,00508
ILMN_2331010	NM_147187	TNFRSF10B	8795	0,000045	0,0051
ILMN_1810229	NM_023001	ARID4A	5926	0,0000464	0,0051
ILMN_1743505	NM_016079	VPS24	51652	0,0000468	0,0051
ILMN_2139761	NM_014988	LIMCH1	22998	0,0000468	0,0051
ILMN_1790710	NM_006930	SKP1A	6500	0,0000473	0,0051
ILMN_1714757	NM_018647	TNFRSF19	55504	0,0000481	0,0051
ILMN_1685286	NM_017607	PPP1R12C	54776	0,0000484	0,0051
ILMN_1810962	NM_002844	PTPRK	5796	0,0000491	0,0051
ILMN_1801516	NM_002081	GPC1	2817	0,0000492	0,0051
ILMN_1696709	NM_133439	TADA2A	6871	0,0000492	0,0051
ILMN_1737964	NM_032558	HIATL1	84641	0,0000493	0,0051
ILMN_1719611	NM_001762	CCT6A	908	0,0000497	0,0051
ILMN_2317923	NM_178031	TMEM132A	54972	0,0000498	0,0051
ILMN_1667417	NM_016277	RAB23	51715	0,0000502	0,00511
ILMN_1728471	NM_006421	ARFGEF1	10565	0,0000504	0,00511
ILMN_2364574	NM_002750	MAPK8	5599	0,0000517	0,00513
ILMN_2190942	NM_030917	FIP1L1	81608	0,0000517	0,00513
ILMN_1658333	NM_004425	ECM1	1893	0,0000522	0,00513
ILMN_1787081	NM_001488	TADA2A	6871	0,0000523	0,00513
ILMN_2103014	NM_080667	CCDC104	112942	0,0000524	0,00513
ILMN_1784408	XR_017961	C8orf48	157773	0,0000527	0,00514
ILMN_1671742	NM_023011	UPF3A	65110	0,0000544	0,00525
ILMN_1755974	NM_005165	ALDOC	230	0,0000552	0,00528
ILMN_1716790	NM_173075	APBB2	323	0,0000557	0,0053
ILMN_1671404	NM_003174	SVIL	6840	0,0000561	0,00532
ILMN_1744534	NM_001001660	LYRM5	144363	0,0000565	0,00532

ILMN_1666715	NM_017778	WHSC1L1	54904	0,000057	0,00533
ILMN_2307598	NM_032295	SLC37A3	84255	0,0000574	0,00533
ILMN_2208491	NR_002775	RPLP0P2	113157	0,0000575	0,00533
ILMN_1712040	NM_005766	FARP1	10160	0,0000591	0,00545
ILMN_3236428	NM_001100829	TMEM170B	1E+08	0,0000625	0,00567
ILMN_3245616	NM_020943	CWC22	57703	0,0000628	0,00567
ILMN_2330213	NM_001913	CUX1	1523	0,0000632	0,00567
ILMN_1739199	NR_003659	FAM39DP	374666	0,0000642	0,00571
ILMN_1679241	NM_175075	C8orf42	157695	0,0000648	0,00572
ILMN_2165473	NM_021242	MID1IP1	58526	0,0000649	0,00572
ILMN_1710170	NM_177526	PPAP2C	8612	0,0000672	0,00583
ILMN_2286334	NM_001080415	SR140	23350	0,0000676	0,00583
ILMN_1813703	NM_152663	RALGPS2	55103	0,0000697	0,00588
ILMN_1742143	NM_021065	HIST1H2AD	3013	0,0000698	0,00588
ILMN_2399140	NM_004583	RAB5C	5878	0,0000698	0,00588
ILMN_3247023	NR_015410	FLJ22536	401237	0,0000702	0,00588
ILMN_1800837	NM_006324	CFDP1	10428	0,0000703	0,00588
ILMN_1716821	NM_031899	GORASP1	64689	0,0000706	0,00588
ILMN_2268381	NM_001042576	RRBP1	6238	0,0000709	0,00588
ILMN_1813314	NM_080593	HIST1H2BK	85236	0,0000709	0,00588
ILMN_2243516	NM_199124	C11orf63	79864	0,0000719	0,0059
ILMN_1784037	NM_001083621	ZBTB40	9923	0,0000726	0,00592
ILMN_1675982	NM_138619	GGA3	23163	0,0000727	0,00592
ILMN_2287147	NM_014233	UBTF	7343	0,000073	0,00592
ILMN_1668378	NM_199344	SFT2D2	375035	0,0000739	0,00592
ILMN_1733964	NM_012204	GTF3C4	9329	0,0000744	0,00592
ILMN_1760509	NM_005442	EOMES	8320	0,0000754	0,00592
ILMN_1701589	NM_004037	AMPD2	271	0,0000758	0,00592
ILMN_3229052	NM_180703	SNRNP35	11066	0,0000765	0,00592
ILMN_1745607	NM_000014	A2M	2	0,0000768	0,00592
ILMN_2345119	NM_181332	NLGN4X	57502	0,0000773	0,00592
ILMN_1778617	NM_001015891	TAF9	6880	0,0000786	0,00594
ILMN_2100693	NM_003010	MAP2K4	6416	0,0000787	0,00594
ILMN_1723962	NM_020169	LXN	56925	0,0000796	0,00594
ILMN_1678968	NM_005261	GEM	2669	0,0000798	0,00594
ILMN_2404903	NM_198389	PDPN	10630	0,00008	0,00594
ILMN_1759984	NM_198991	KCTD1	284252	0,0000803	0,00594
ILMN_1808196	NM_004832	GSTO1	9446	0,0000806	0,00594
ILMN_2151739	NM_001752	CAT	847	0,0000809	0,00594
ILMN_2098119	NM_005414	SKIL	6498	0,0000811	0,00594
ILMN_3247906	NM_018683	RNF114	55905	0,0000815	0,00595
ILMN_2226628	NM_007149	ZNF184	7738	0,0000823	0,00598
ILMN_1658709	NM_002291	LAMB1	3912	0,0000847	0,00609
ILMN_2193325	NM_006983	MMP23B	8510	0,0000864	0,00614
ILMN_2233493	NM_022913	GPBP1	65056	0,0000866	0,00614
ILMN_1688452	NM_016309	LCMT1	51451	0,0000876	0,00616
ILMN_2331062	NM_005093	CBFA2T2	9139	0,0000891	0,00621
ILMN_1731788	NM_013959	NRG1	3084	0,0000897	0,00621
ILMN_1690174	NM_019074	DLL4	54567	0,0000901	0,00621
ILMN_1686414	NM_024824	ZC3H14	79882	0,0000901	0,00621

ILMN_1668246	NM_178545	TMEM52	339456	0,0000913	0,00621
ILMN_2415357	NM_175863	ARID1B	57492	0,0000917	0,00621
ILMN_1804113	NM_003721	RFXANK	8625	0,0000919	0,00621
ILMN_1794782	NM_016818	ABCG1	9619	0,0000924	0,00621
ILMN_3236942	NR_002919	SNORA5A	654319	0,0000927	0,00621
ILMN_2404665	NM_033093	TRIM5	85363	0,000093	0,00621
ILMN_2225348	NM_001023563	ZNF805	390980	0,0000934	0,00621
ILMN_1805792	NM_007118	TRIO	7204	0,0000945	0,00626
ILMN_1794692	NM_006892	DNMT3B	1789	0,0000977	0,00639
ILMN_1689162	NM_022899	ACTR8	93973	0,0000983	0,00639
ILMN_1666777	NM_006884	SHOX2	6474	0,000099	0,0064
ILMN_2134381	NR_002808	C14orf85	319085	0,0001	0,00642
ILMN_2360710	NM_001018004	TPM1	7168	0,0001008	0,00642
ILMN_1710543	NM_144564	SLC39A3	29985	0,0001009	0,00642
ILMN_1752409	NM_014494	TNRC6A	27327	0,0001051	0,0066
ILMN_3242011	NM_018221	MOBKL1B	55233	0,0001051	0,0066
ILMN_2294644	NM_022457	RFWD2	64326	0,0001059	0,00663
ILMN_2183261	NM_015963	THAP4	51078	0,0001064	0,00664
ILMN_1750088	NM_006296	VRK2	7444	0,0001096	0,00667
ILMN_1745110	NM_014713	LAPTM4A	9741	0,0001101	0,00667
ILMN_1656409	NM_172311	STON1-GTF2A1L	286749	0,0001103	0,00667
ILMN_2263466	NM_000018	ACADVL	37	0,0001105	0,00667
ILMN_2399328	NM_015456	COBRA1	25920	0,0001106	0,00667
ILMN_2220518	NM_006402	HBXIP	10542	0,0001107	0,00667
ILMN_1652472	NM_004333	BRAF	673	0,0001109	0,00667
ILMN_1813027	NM_033549	TRIM41	90933	0,0001111	0,00667
ILMN_1736847	NM_001001654	MED8	112950	0,0001117	0,00668
ILMN_1758658	NM_003824	FADD	8772	0,000113	0,00668
ILMN_1657665	NM_016620	ZNF644	84146	0,0001137	0,00668
ILMN_2280135	NM_001017974	P4HA2	8974	0,0001147	0,00669
ILMN_1661674	NM_014000	VCL	7414	0,0001162	0,0067
ILMN_1807919	NM_022648	TNS1	7145	0,0001167	0,0067
ILMN_1708486	NM_004368	CNN2	1265	0,0001171	0,0067
ILMN_1676413	NM_003385	VSNL1	7447	0,0001171	0,0067
ILMN_1674421	NM_014742	TM9SF4	9777	0,0001172	0,0067
ILMN_3309279	NR_003234	SNORD113-6	767566	0,0001184	0,00672
ILMN_1761175	NM_003952	RPS6KB2	6199	0,0001192	0,00672
ILMN_1662910	NM_030971	SFXN3	81855	0,0001208	0,00672
ILMN_2151114	NM_003385	VSNL1	7447	0,000121	0,00672
ILMN_3247148	NR_003942	SNORD76	692196	0,0001211	0,00672
ILMN_1703955	NM_148177	FBXO32	114907	0,0001212	0,00672
ILMN_1810584	NM_000877	IL1R1	3554	0,0001215	0,00672
ILMN_1682501	NM_206999	CNOT1	23019	0,0001215	0,00672
ILMN_2285213	NM_006736	DNAJB2	3300	0,0001232	0,00677
ILMN_1739573	NM_014494	TNRC6A	27327	0,0001252	0,00681
ILMN_1701402	NM_153687	IKBIP	121457	0,0001253	0,00681
ILMN_2290808	NM_000982	RPL21	6144	0,0001261	0,00683
ILMN_1680419	NM_024708	ASB7	140460	0,0001265	0,00683
ILMN_1760143	NM_175573	ADRM1	11047	0,0001266	0,00683
ILMN_2126239	NM_015327	SMG5	23381	0,0001284	0,00687

ILMN_2064694	NM_003156	STIM1		6786	0,0001288	0,00688
ILMN_1661156	NM_020718	USP31		57478	0,0001293	0,00688
ILMN_1748881	NM_012219	MRAS		22808	0,0001304	0,00692
ILMN_1738326	NM_004846	EIF4E2		9470	0,0001309	0,00693
ILMN_1696004	NM_024652	LRRK1		79705	0,0001317	0,00694
ILMN_1772216	NM_005676	RBM10		8241	0,0001321	0,00694
ILMN_1792669	NM_000411	HLCS		3141	0,0001349	0,00704
ILMN_1679021	NM_020418	PCBP4		57060	0,000135	0,00704
ILMN_2343332	NM_016283	TAF9		6880	0,0001378	0,00714
ILMN_1745130	NM_001082576	RBM9		23543	0,000138	0,00714
ILMN_1714511	NM_004562	PARK2		5071	0,0001381	0,00714
ILMN_1750145	NM_012479	YWHAG		7532	0,0001384	0,00714
ILMN_2347999	NM_207584	IFNAR2		3455	0,0001392	0,00715
ILMN_3241139	NR_002738	SNORD57		26792	0,00014	0,00717
ILMN_1701596	NM_001023	RPS20		6224	0,0001412	0,00718
ILMN_1714569	NM_006201	PCTK1		5127	0,0001432	0,00718
ILMN_1709860	NM_001039675	UNC45A		55898	0,0001436	0,00718
ILMN_1760830	NM_148177	FBXO32		114907	0,0001441	0,00718
ILMN_2189458	NM_018130	SHQ1		55164	0,0001442	0,00718
ILMN_3251227	NM_014346	TBC1D22A		25771	0,0001445	0,00718
ILMN_2206474	NM_024893	TMEM90B		79953	0,0001451	0,00718
ILMN_1665357	NM_001981	EPS15		2060	0,0001452	0,00718
ILMN_2225974	NM_002061	GCLM		2730	0,0001465	0,00721
ILMN_1762801	NM_007249	KLF12		11278	0,0001486	0,00724
ILMN_1753468	NM_001040034	CD63		967	0,0001486	0,00724
ILMN_2225135	NM_001490	GCNT1		2650	0,0001492	0,00724
ILMN_1689177	NM_001030059	PPAPDC1A		196051	0,0001509	0,00729
ILMN_3248232	NR_002950	SNORA2A		677793	0,0001535	0,00738
ILMN_1699384	NM_006245	PPP2R5D		5528	0,0001538	0,00738
ILMN_1763436	NM_015046	SETX		23064	0,0001546	0,0074
ILMN_1775045	NM_004797	ADIPOQ		9370	0,0001602	0,00765
ILMN_1743208	NM_152905	NEDD1		121441	0,0001607	0,00765
ILMN_1802799	NM_024595	AKIRIN1		79647	0,0001619	0,00767
ILMN_1677038	NM_024913	FLJ21986		79974	0,0001624	0,00768
ILMN_1706521	NM_001319	CSNK1G2		1455	0,0001628	0,00768
ILMN_3243527	NM_001005464	HIST2H3A		333932	0,0001635	0,00768
ILMN_1696883	NM_001081550	THOC2		57187	0,0001643	0,00768
ILMN_1774689	NM_006765	TUSC3		7991	0,0001666	0,00777
ILMN_1761969	NM_016041	DERL2		51009	0,0001696	0,00785
ILMN_1768953	NM_002997	SDC1		6382	0,0001703	0,00787
ILMN_3243390	NM_001099269	ZNF506		440515	0,0001715	0,00791
ILMN_1725612	NM_007172	NUP50		10762	0,000172	0,00791
ILMN_1712936	NM_013329	C21orf66		94104	0,0001778	0,00804
ILMN_1681798	NM_145800		41888	23157	0,0001781	0,00804
ILMN_1736184	NM_000849	GSTM3		2947	0,0001794	0,00807
ILMN_1651692	NM_005990	STK10		6793	0,0001826	0,00813
ILMN_2218277	NM_002952	RPS2		6187	0,000183	0,00813
ILMN_1727992	NM_022549	FEZ1		9638	0,0001831	0,00813
ILMN_2124352	NM_032299	DCUN1D5		84259	0,0001845	0,00814
ILMN_1746968	NM_024165	PHF1		5252	0,0001848	0,00814

ILMN_1793241	NM_001047	SRD5A1	6715	0,000186	0,00817
ILMN_1765363	NM_024423	DSC3	1825	0,0001872	0,0082
ILMN_1652456	NM_015544	TMEM98	26022	0,0001911	0,00826
ILMN_1796126	NM_198530	MXRA7	439921	0,0001931	0,00831
ILMN_1687782	NM_133340	RAD17	5884	0,0001938	0,00831
ILMN_1725108	NM_031953	SNX25	83891	0,0001957	0,00831
ILMN_1725700	NM_020963	MOV10	4343	0,0001971	0,00835
ILMN_2330570	NM_001003680	LEPR	3953	0,0001993	0,00837
ILMN_1811277	NM_213590	TRIM13	10206	0,0001998	0,00837
ILMN_1680727	NM_016066	GLRX2	51022	0,0002002	0,00837
ILMN_2298511	NM_001031827	BOLA2	552900	0,0002007	0,00837
ILMN_1692785	NM_014851	KLHL21	9903	0,0002009	0,00837
ILMN_1693523	NR_003675	LOC441046	441046	0,0002013	0,00837
ILMN_1807563	NM_004470	FKBP2	2286	0,0002022	0,00839
ILMN_2260813	NM_022117	TSPYL2	64061	0,0002039	0,00839
ILMN_2380101	NM_023923	PHACTR4	65979	0,0002041	0,00839
ILMN_3251751	NM_152778	MFSD8	256471	0,0002045	0,00839
ILMN_1744387	NM_001034838	KCNIP1	30820	0,0002047	0,00839
ILMN_1755047	NM_024512	LRRC2	79442	0,0002048	0,00839
ILMN_1664416	NM_002399	MEIS2	4212	0,0002064	0,00844
ILMN_1709486	NM_006307	SRPX	8406	0,0002086	0,0085
ILMN_1675898	NM_004844	SH3BP5	9467	0,0002102	0,00852
ILMN_2401769	NM_001007157	PHF14	9678	0,0002118	0,00854
ILMN_1813379	NM_001561	TNFRSF9	3604	0,0002128	0,00856
ILMN_1729775	NM_015560	OPA1	4976	0,0002131	0,00856
ILMN_1788700	NM_198526	ZNF710	374655	0,0002147	0,00858
ILMN_2409876	NM_153480	IL17RE	132014	0,0002153	0,00858
ILMN_3237665	NM_004718	COX7A2L	9167	0,0002158	0,00858
ILMN_1771149	NM_014763	MRPL19	9801	0,0002166	0,00858
ILMN_2346831	NM_001015883	MGAT2	4247	0,0002166	0,00858
ILMN_2337241	NM_001019	RPS15A	6210	0,0002172	0,00858
ILMN_2333594	NM_001005849	SUMO2	6613	0,0002175	0,00858
ILMN_1807031	NM_001017923	C14orf28	122525	0,000219	0,00861
ILMN_2055781	NM_016523	KLRF1	51348	0,0002194	0,00861
ILMN_1743847	NM_030649	ACAP3	116983	0,0002198	0,00861
ILMN_1678353	NM_005766	FARP1	10160	0,0002235	0,00868
ILMN_1758315	NM_173653	SLC9A9	285195	0,0002241	0,00869
ILMN_1800935	NM_022786	ARV1	64801	0,000225	0,00869
ILMN_1719975	NM_014620	HOXC4	3221	0,0002253	0,00869
ILMN_2200917	NM_003615	SLC4A7	9497	0,0002259	0,00869
ILMN_1750160	NM_024091	FASTKD3	79072	0,0002282	0,00875
ILMN_1656293	NM_004287	GOSR2	9570	0,0002286	0,00875
ILMN_1806809	NM_003452	ZNF189	7743	0,00023	0,00877
ILMN_1804137	NM_001010986	ATP11C	286410	0,0002311	0,00878
ILMN_1775759	NM_002524	NRAS	4893	0,0002332	0,00884
ILMN_1654322	NM_001679	ATP1B3	483	0,0002346	0,00886
ILMN_1797209	NM_018718	TSGA14	95681	0,0002402	0,009
ILMN_1669023	NM_020482	FHL5	9457	0,0002437	0,00905
ILMN_3243890	NM_002488	NDUFA2	4695	0,0002465	0,00909
ILMN_1742808	NM_201997	SF1	7536	0,0002465	0,00909

ILMN_2318568	NM_001002018	HCFC1R1	54985	0,0002483	0,00911
ILMN_1747673	NM_001007279	RASL10A	10633	0,0002524	0,00919
ILMN_1751589	NM_145266	NUDCD2	134492	0,0002544	0,00922
ILMN_1694877	NM_001226	CASP6	839	0,0002554	0,00923
ILMN_2321634	NM_133340	RAD17	5884	0,0002561	0,00924
ILMN_2147133	NM_173638	NBPF15	284565	0,0002579	0,00928
ILMN_1719254	NM_015163	TRIM9	114088	0,0002609	0,00931
ILMN_2062370	NM_017948	NOL8	55035	0,0002611	0,00931
ILMN_1665515	NM_052871	MGC4677	112597	0,0002639	0,00932
ILMN_2293692	NM_004380	CREBBP	1387	0,0002645	0,00932
ILMN_2394242	NM_001025580	AMMECR1	9949	0,0002647	0,00932
ILMN_3265365	NM_032171	CEP78	84131	0,000265	0,00932
ILMN_1745119	NM_138701	C7orf11	136647	0,0002705	0,00943
ILMN_1754746	NM_033031	CCNB3	85417	0,0002736	0,00947
ILMN_1815361	NM_001167	XIAP	331	0,0002741	0,00947
ILMN_3237044	NR_000017	SNORD36B	26814	0,0002746	0,00947
ILMN_1697790	NM_006411	AGPAT1	10554	0,000278	0,00955
ILMN_1660433	NM_175863	ARID1B	57492	0,0002782	0,00955
ILMN_1749709	NM_019056	NDUFB11	54539	0,0002805	0,00957
ILMN_1664231	NM_006327	TIMM23	10431	0,0002808	0,00957
ILMN_1805766	NM_002702	POU6F1	5463	0,000282	0,00958
ILMN_1667771	NM_001001550	GRB10	2887	0,0002836	0,00959
ILMN_1800451	NM_005481	MED16	10025	0,0002836	0,00959
ILMN_1756469	NM_000156	GAMT	2593	0,0002852	0,00961
ILMN_1741566	NM_001719	BMP7	655	0,0002857	0,00961
ILMN_1732296	NM_002167	ID3	3399	0,0002866	0,00961
ILMN_1787308	NM_024779	PIP4K2C	79837	0,0002867	0,00961
ILMN_2398664	NM_025126	RNF34	80196	0,0002909	0,0097
ILMN_1796976	NM_021209	NLRC4	58484	0,0002921	0,0097
ILMN_1665167	NM_134260	RORA	6095	0,0002922	0,0097
ILMN_2192620	NM_138353	DCAF15	90379	0,0002955	0,00978
ILMN_2084031	NM_173814	PRTG	283659	0,0003016	0,00988
ILMN_2068747	NM_000274	OAT	4942	0,0003031	0,00991
ILMN_1757736	NM_005853	IRX5	10265	0,0003039	0,00991
ILMN_2070043	NM_152542	PPM1K	152926	0,000304	0,00991
ILMN_1654890	NM_052925	LENG8	114823	0,0003067	0,00997
ILMN_1705562	NM_015210	KIAA0802	23255	0,0003084	0,00999

T patients

Permutation p-value	Fold-change mutated vs wt DT
Permutation p-v:	Fold-change
< 1e-07	2,12
< 1e-07	2,34
< 1e-07	2,19
< 1e-07	2,63
< 1e-07	3,19
< 1e-07	2,53
< 1e-07	2,21
< 1e-07	3,14
< 1e-07	2,31
< 1e-07	2,25
< 1e-07	2,38
< 1e-07	2,22
< 1e-07	2,05
< 1e-07	3,4
< 1e-07	2,27
< 1e-07	2,66
< 1e-07	2,05
< 1e-07	2,11
< 1e-07	2,25
< 1e-07	3,66
0,0001	2,94
< 1e-07	3,87
< 1e-07	2,37
< 1e-07	2,11
< 1e-07	2,27
< 1e-07	2,84
< 1e-07	2,13
< 1e-07	0,48
< 1e-07	2,46
< 1e-07	2,61
< 1e-07	2,13
0,0001	5,35
< 1e-07	2,92
< 1e-07	0,43
< 1e-07	3,06
0,0001	3,2
< 1e-07	3,14
< 1e-07	2,92
< 1e-07	3,76
< 1e-07	2,24
< 1e-07	2,54
< 1e-07	3,49
< 1e-07	2,25
< 1e-07	3,22
< 1e-07	2,85

< 1e-07		2,6
< 1e-07		2,21
< 1e-07		2,71
< 1e-07		2,96
< 1e-07		2,21
< 1e-07		2,9
< 1e-07		2,04
< 1e-07		2,46
< 1e-07		2,95
< 1e-07		2,67
< 1e-07		2,29
< 1e-07		3,13
< 1e-07		2,13
< 1e-07		2,51
< 1e-07		3,77
	0,0001	2,17
< 1e-07		2,13
	0,0001	2,55
< 1e-07		4,76
< 1e-07		2,35
< 1e-07		2,15
< 1e-07		0,46
	0,0002	2,16
< 1e-07		2,46
	0,0001	2,43
< 1e-07		2,7
< 1e-07		2,77
< 1e-07		0,26
< 1e-07		0,47
< 1e-07		0,43
< 1e-07		2,48
< 1e-07		3,61
< 1e-07		2,11
< 1e-07		2,35
< 1e-07		2,76
< 1e-07		0,43
< 1e-07		2,26
< 1e-07		2,92
< 1e-07		2,64
< 1e-07		3,57
< 1e-07		2,09
< 1e-07		3,1
< 1e-07		3,59
< 1e-07		2,06
< 1e-07		2,64
< 1e-07		2,42
< 1e-07		0,46
	0,0001	2,26
	0,0001	3,42
< 1e-07		2,36

< 1e-07		2,67
< 1e-07		3,2
< 1e-07		2,32
< 1e-07		0,5
< 1e-07		0,31
< 1e-07		2,31
	0,0001	2,23
< 1e-07		3,04
< 1e-07		2,96
< 1e-07		3,48
< 1e-07		2,93
	0,0001	2,83
< 1e-07		2,81
	0,0002	2,11
< 1e-07		0,27
< 1e-07		2
< 1e-07		2,63
< 1e-07		2,72
< 1e-07		2,35
< 1e-07		3,74
< 1e-07		3,24
< 1e-07		2,19
< 1e-07		2,45
	0,0002	2,78
	0,0001	3,85
	0,0001	2,44
	0,0002	2,49
< 1e-07		0,38
	0,0002	2,94
< 1e-07		2,74
< 1e-07		2,43
	0,0001	3,1
	0,0001	4,07
	0,0003	2,14
< 1e-07		2,49
< 1e-07		2,12
< 1e-07		2,93
	0,0001	2,2
< 1e-07		2,29
	0,0001	2,54
< 1e-07		2,79
	0,0001	2,46
	0,0001	3,5
< 1e-07		2,69
< 1e-07		2,03
	0,0001	2,47
< 1e-07		0,34
< 1e-07		2,38
< 1e-07		0,43
< 1e-07		0,41

< 1e-07		2,33
< 1e-07		2,73
< 1e-07		2,27
< 1e-07		3,01
< 1e-07		0,45
< 1e-07		2,65
	0,0001	3,34
	0,0001	2,53
< 1e-07		2,4
< 1e-07		0,43
	0,0001	2,77
< 1e-07		2,85
< 1e-07		3,32
	0,0002	3
	0,0001	2,13
	0,0002	2,12
< 1e-07		2,09
	0,0001	2,94
< 1e-07		2,07
	0,0001	2,93
< 1e-07		2,28
< 1e-07		2,44
< 1e-07		2,53
	0,0001	2,1
< 1e-07		2,54
< 1e-07		2,07
< 1e-07		0,29
	0,0003	3,36
< 1e-07		2,52
< 1e-07		0,41
	0,0002	4,34
	0,0001	2,72
< 1e-07		2,26
< 1e-07		2,43
	0,0001	2,5
	0,0004	3,71
	0,0003	2,78
	0,0002	2,09
	0,0002	0,4
	0,0001	2,33
< 1e-07		2,25
	0,0001	2,47
< 1e-07		2,05
< 1e-07		3,4
< 1e-07		2,43
	0,0001	2,28
< 1e-07		2,08
	0,0002	3,14
	0,0002	2,32
	0,0001	2,15

< 1e-07		0,23
< 1e-07		2,21
	0,0001	2,06
	0,0001	0,46
	0,0001	2,91
	0,0001	2,37
< 1e-07		3,12
	0,0001	2,36
	0,0002	2,2
	0,0002	2,01
	0,0002	2,13
< 1e-07		2,07
	0,0002	2,31
< 1e-07		2,35
	0,0003	3,31
	0,0002	2,8
< 1e-07		2,22
	0,0001	2,43
< 1e-07		2,33
	0,0002	2,13
	0,0003	2,92
	0,0002	3,27
	0,0003	2,63
	0,0001	2,99
	0,0001	2,13
	0,0003	2,26
< 1e-07		2,24
	0,0002	2,09
< 1e-07		2,94
< 1e-07		3,5
< 1e-07		2,72
	0,0001	0,47
	0,0002	3,87
	0,0003	2,21
	0,0001	2,33
	0,0002	3,43
	0,0001	2,44
	0,0001	2,37
	0,0001	2,92
< 1e-07		2,12
	0,0001	0,46
	0,0002	3,13
	0,0001	2,19
	0,0002	2,79
	0,0001	2,53
	0,0002	2,68
	0,0001	2,39
	0,0003	2,51
	0,0002	2,53
	0,0002	0,47

0,0003	2,07
0,0003	2,63
0,0001	2,14
0,0001	2,06
0,0003	2,06
0,0002	2,14
< 1e-07	2,46
0,0001	3,02
0,0002	2,96
0,0002	2,14
0,0004	0,35
0,0001	2,61
0,0005	2,49
0,0002	2,09
0,0003	2,8
0,0002	2,23
< 1e-07	2,79
0,0003	0,29
0,0001	2,38
0,0001	2,82
0,0004	2,6
0,0002	0,48
< 1e-07	2,45
0,0006	3,35
< 1e-07	2,09
0,0004	2,46
0,0002	2,55
0,0001	2,54
0,0007	3,32
0,0002	2,01
0,0004	0,27
0,0003	3,17
0,0001	2
0,0001	0,42
0,0002	2,14
0,0002	3,78
0,0005	2,65
0,0002	3,95
0,0001	2,49
0,0003	2,31
0,0001	2,72
0,0006	2,69
0,0004	2,42
0,0003	2,35
0,0001	0,47
0,0003	2,38
< 1e-07	2,06
0,0002	2,14
0,0004	2,57
0,0002	2,93

< 1e-07		0,41
< 1e-07		2,74
	0,0001	2,47
< 1e-07		2,06
	0,0003	2,97
	0,0003	2,28
	0,0004	2,27
< 1e-07		0,38
	0,0003	2,05
	0,0003	2,09
	0,0003	2,18
	0,0005	0,45
< 1e-07		0,36
	0,0003	3,08
	0,0002	2,25
	0,0002	2,04
	0,0001	2,42
	0,0004	0,35
	0,0003	0,26
	0,0002	2,62
< 1e-07		0,5
	0,0004	2,63
	0,0002	2,06
	0,0003	3,07
	0,0001	2,24
	0,0002	3,12
	0,0003	0,3
< 1e-07		2,22
	0,0005	2,08
	0,0003	2,39
	0,0004	2,31
	0,0003	2,11
< 1e-07		0,48
	0,0005	3,38
	0,0001	2,72
	0,0001	2,99
	0,0004	2,08
	0,0003	3,61
	0,0003	2,32
	0,0002	0,49
	0,0003	2,06
	0,0002	2,59
	0,0004	2,3
	0,0003	2,25
	0,0004	2,68
	0,0004	2,01
	0,0002	2,17
	0,0002	0,31
	0,0001	2,12
	0,0004	2,37

	0,0003	3,63
	0,0002	0,36
	0,0005	2,02
	0,0006	2,36
	0,0004	3,47
< 1e-07		2,08
	0,0004	2,36
	0,0002	2,34
	0,0001	2,85
	0,0005	2,06
	0,0005	2,13
	0,0003	2,25
	0,0002	2,17
	0,0001	0,26
	0,0009	2,08
< 1e-07		2,5
	0,0002	2,64
	0,0007	2,46
	0,0003	2,41
	0,0003	2,36
	0,0001	2,16
	0,0003	2,43
	0,0003	2,16
	0,0002	0,41
	0,0001	2,49
	0,0003	2,86
< 1e-07		0,49
	0,0005	2,15
	0,0005	0,32
	0,0004	3,02
	0,0001	2,57
	0,0001	0,38
	0,0003	2,8
	0,0006	2,97
< 1e-07		2,14
	0,0002	2,28
	0,0002	2,58

Computational details

The Amber ff14SB force field (1) was used to parameterize all protein structures. All simulations were carried out using the *Pmemd* modules of Amber 14 (2), running on a hybrid CPU/GPU calculation cluster.

The optimized full-length three-dimensional (3D) models of wt and mutant isoforms of β-catenin were obtained by a combination of homology modeling techniques and molecular dynamics refinements. The protein model was built starting from the available structures of the phosphorylation motif (aa. Lys19-Pro44, 2G57.pdb (3); aa. Asp83-Gln143, 4ONS.pdb (4)), and of the armadillo repeats domain with part of the protein C-terminal (2Z6H.pdb (5)). The models of the T41A and S45F variant proteins were obtained by mutating the relevant amino acids, and optimizing the corresponding isoforms via energy relaxation followed by MD simulations in solution in agreement with a well-validated computational procedure (6).

The α-catenin/β-catenin protein-protein interface and the docking modes of α-catenin (4IGG.pdb, (7)) onto the β-catenin WT and its two truncated isoforms were determined using the HADDOCK server (8). The resulting protein/protein docked conformations were clustered and visualized; then, the structure of each complex characterized by the lowest interaction energy in the prevailing cluster was selected for further modeling (6). The selected α-catenin/β-catenin complexes were then solvated in a TIP3P (9) water box and, then, the required amount of Na^+ and Cl^- ions were added to neutralize the system and to mimic physiological salt conditions (150 mM), removing eventual overlapping water molecules. The solvated systems were subjected to a combination of steepest descent/conjugate gradient minimization of the potential energy, during which all bad contacts were relieved. The relaxed systems were then gradually heated to 300 K in three intervals by running constant volume-constant temperature (NVT) MD simulation, allowing a 0.5 ns interval per 100 K. Subsequently, 40 ns MD simulations under isobaric-isothermal (NPT) conditions were conducted to fully equilibrate each solvated compound. The *SHAKE* algorithm (10) with a geometric tolerance of $5x10^{-4}$ Å was imposed on all covalent bonds involving hydrogen atoms. Temperature control was achieved using the Langevin temperature equilibration scheme and an integration time step of 2 fs. The particle mesh Ewald (PME) method (11) was used to treat the long-range electrostatics. At this point, these MD runs were followed by other 200 ns of NVT MD simulation. The last 100 ns of the MD data collection period described were used for the calculation of the binding free energy between the two proteins via the MM/PBSA (Molecular Mechanincs/Poisson Boltzmann Surface Area) approach (6).

According to this theory, the free energy of binding (ΔG_{bind}) between α-catenin and each β-catenin variant can be calculated as the sum of different energetic contributions, corresponding to the

average MD energies ($\Delta E_{MM} = \Delta E_{ele} + \Delta E_{vdW}$), the average solvation free energy ($\Delta G_{solv} = \Delta G_{solv,pol} + \Delta G_{solv,nonpol}$), and the entropic contribution ($-T\Delta S$).

Table SI1. Binding free energies (ΔG_{bind}) and binding free energy differences ($\Delta\Delta G_{bind}$) for the wt, T41A and S45F β-catenin in complex with α-catenin.

	ΔG_{bind} (kcal/mol)	$\Delta\Delta G_{bind}$ (kcal/mol)
WT	-13.15 ± 0.26	-
T41A	-10.41 ± 0.28	-2.74
S45F	-10.28 ± 0.28	-2.87

References

1. Maier JA, Martinez C, Kasavajhala K, Wickstrom L, Hauser KE, Simmerling C. ff14SB: improving the accuracy of protein side chain and backbone parameters from ff99SB. J Chem Theory Comput. 2015;11(8): 3696-13.

2. Case DA, Babin, V, Berryman JT, Betz RM, Cai Q, Cerutti DS, et al. AMBER 14, University of California, San Francisco, CA, USA, 2014.

3. Megy S, Bertho G, Gharbi-Benarous J, Baleux F, Benarous R, Girault JP. STD and TRNOESY NMR studies for the epitope mapping of the phosphorylation motif of the oncogenic protein beta-catenin recognized by a selective monoclonal antibody. Febs Lett. 2006;580:5411-22.

4. Pokutta S, Choi HJ, Ahlsen G, Hansen SD, Weis WI. Structural and thermodynamic characterization of cadherin·β-catenin·α-catenin complex formation. J Biol Chem. 2014;289(19):13589-601.

5. Xing Y, Takemaru K, Liu J, Berndt JD, Zheng JJ, Moon RT, Xu W. Crystal structure of a full-length beta-catenin. Structure. 2008;16(3):478-87.

(6) a) Morgan A, Gandin I, Belcaro C, Palumbo P, Palumbo O, Biamino E, Dal Col V, Laurini E, Pricl S, Bosco P, Carella M, Ferrero GB, Romano C, d'Adamo AP, Faletra F, Vozzi D. Target sequencing approach intended to discover new mutations in non-syndromic intellectual disability. Mutat Res. 2015;781:32-6; b) Brambilla L, Genini D, Laurini E, Merulla J, Perez L, Fermeglia M, Carbone GM, Pricl S, Catapano CV. Hitting the right spot: Mechanism of action of OPB-31121, a novel and potent inhibitor of the Signal Transducer and Activator of Transcription 3 (STAT3). Mol Oncol. 2015;9(6):1194-206; c) Pricl S, Cortelazzi B, Dal Col V, Marson D, Laurini E, Fermeglia M, Licitra L, Pilotti S, Bossi P, Perrone F. Smoothened (SMO) receptor mutations dictate resistance to vismodegib in basal cell carcinoma. Mol Oncol. 2015;9(2):389-97; d) Brune S, Schepmann D, Klempnauer KH, Marson D, Dal Col V, Laurini E, Fermeglia M, Wünsch B, Pricl S. The sigma enigma: in vitro/in silico site-directed mutagenesis studies unveil σ1 receptor ligand binding. Biochemistry. 2014;53(18):2993-3003; e) Gibbons DL, Pricl S, Posocco P, Laurini E, Fermeglia M, Sun H, Talpaz M, Donato N, Quintás-Cardama A. Molecular dynamics reveal BCR-ABL1 polymutants as a unique mechanism of resistance to PAN-BCR-ABL1 kinase inhibitor therapy.

Proc Natl Acad Sci U S A. 2014;111(9):3550-5; f) Bozzi F, Conca E, Laurini E, Posocco P, Lo Sardo A, Jocollè G, Sanfilippo R, Gronchi A, Perrone F, Tamborini E, Pelosi G, Pierotti MA, Maestro R, Pricl S, Pilotti S. In vitro and in silico studies of MDM2/MDMX isoforms predict Nutlin-3A sensitivity in well/de-differentiated liposarcomas. Lab Invest. 2013;93(11):1232-40; g) Conca E, Miranda C, Dal Col V, Fumagalli E, Pelosi G, Mazzoni M, Fermeglia M, Laurini E, Pierotti MA, Pilotti S, Greco A, Pricl S, Tamborini E. Are two better than one? A novel double-mutant KIT in GIST that responds to Imatinib. Mol Oncol. 2013;7(4):756-62; h) Gibbons DL, Pricl S, Kantarjian H, Cortes J, Quintás-Cardama A. The rise and fall of gatekeeper mutations? The BCR-ABL1 T315I paradigm. Cancer. 2012;118(2):293-9; i) Pierotti MA, Tamborini E, Negri T, Pricl S, Pilotti S. Targeted therapy in GIST: in silico modeling for prediction of resistance. Nat Rev Clin Oncol. 2011;8(3):161-70; j) Dileo P, Pricl S, Tamborini E, Negri T, Stacchiotti S, Gronchi A, Posocco P, Laurini E, Coco P, Fumagalli E, Casali PG, Pilotti S. Imatinib response in two GIST patients carrying two hitherto functionally uncharacterized PDGFRA mutations: an imaging, biochemical and molecular modeling study. Int J Cancer. 2011;128(4):983-90; k) Carta A, Pricl S, Piras S, Fermeglia M, La Colla P, Loddo R. Activity and molecular modeling of a new small molecule active against NNRTI-resistant HIV-1 mutants. Eur J Med Chem. 2009;44(12):5117-22; l) Conca E, Negri T, Gronchi A, Fumagalli E, Tamborini E, Pavan GM, Fermeglia M, Pierotti MA, Pricl S, Pilotti S. Activate and resist: L576P-KIT in GIST. Mol Cancer Ther. 2009;8(9):2491-5; m) Woodman SE, Trent JC, Stemke-Hale K, Lazar AJ, Pricl S, Pavan GM, Fermeglia M, Gopal YN, Yang D, Podoloff DA, Ivan D, Kim KB, Papadopoulos N, Hwu P, Mills GB, Davies MA; n) McAuliffe JC, Wang WL, Pavan GM, Pricl S, Yang D, Chen SS, Lazar AJ, Pollock RE, Trent JC. Unlucky number 13? Differential effects of KIT exon 13 mutation in gastrointestinal stromal tumors. Mol Oncol. 2008;2(2):161-3; o) Negri T, Pavan GM, Virdis E, Greco A, Fermeglia M, Sandri M, Pricl S, Pierotti MA, Pilotti S, Tamborini E. T670X KIT mutations in gastrointestinal stromal tumors: making sense of missense. J Natl Cancer Inst. 2009;101(3):194-204; p) Ferrone M, Perrone F, Tamborini E, Paneni MS, Fermeglia M, Suardi S, Pastore E, Delia D, Pierotti MA, Pricl S, Pilotti S. Functional analysis and molecular modeling show a preserved wild-type activity of p53(C238Y). Mol Cancer Ther. 2006;5(6):1467-73; q) Tamborini E, Pricl S, Negri T, Lagonigro MS, Miselli F, Greco A, Gronchi A, Casali PG, Ferrone M, Fermeglia M, Carbone A, Pierotti MA, Pilotti S. Functional analyses and molecular modeling of two c-Kit mutations responsible for imatinib secondary resistance in GIST patients. Oncogene. 2006;25(45):6140-6; r) Pricl S, Fermeglia M, Ferrone M, Tamborini E. T315I-mutated Bcr-Abl in chronic myeloid leukemia and imatinib: insights from a computational study. Mol Cancer Ther. 2005;4(8):1167-74.

7. Rangarajan ES, Izard T. Dimer asymmetry defines α-catenin interactions. Nat Struct Mol Biol. 2013;20(2):188-93.

8. Dominguez C, Boelens R, Bonvin AMJJ. HADDOCK: a protein-protein docking approach based on biochemical or biophysical information. J Am Chem Soc. 2003;125:1731-7.

9. Jorgensen WL, Chandrasekhar J, Madura JD, Impey RW, Klein ML. Comparison of simple potential functions for simulating liquid water. J Chem Phys. 1983;79:926-35.

10. Ryckaert JP, Ciccotti G, Berendsen HJC. Numerical integration of the Cartesian equations of motion of a system with constraints: molecular dynamics of n-alkanes.

11. Toukmaji A, Sagui C, Board J, Darden T. Efficient particle-mesh Ewald based approach to fixed and induced dipolar interactions. J Chem Phys 2000;113:10913-27.